# Making survival spatial: an integrated model for territory occupancy and capture-recapture data

Jaume A. Badia-Boher[1]*, Michael Schaub[1], Mátyás Prommer[2,3], Marc Kéry[1]

[1]Population Biology Research Unit, Swiss Ornithological Institute, Sempach, Switzerland

[2]Wildlife Ecology and Conservation, University of Florida, Gainesville, Florida, USA

[3]MME-BirdLife Hungary, Budapest, Hungary

*Corresponding author: jaume.badia@vogelwarte.ch

**Data and Code:** will be provided publicly in the published version of the article. For previous access, please contact the corresponding author.

**Abstract**

1. Knowledge about spatial variation in survival is central to understanding population dynamics and guiding conservation, yet assessing it is very hard. This limitation arises because capture-mark-recapture (CMR) data required for such inference must be collected over large spatial extents, which is logistically demanding and seldom possible. By contrast, territory occupancy (TO) data are typically spatially rich and widely available for territorial species, but they do not directly inform individual survival.
2. We developed an integrated model combining CMR and TO data. The model links site-level occupancy dynamics, governed by site persistence and colonization probabilities, to survival of the territory owner, allowing both data sources to jointly inform spatiotemporal variation in survival. To accommodate potential violations of this

deterministic occupancy-survival link arising from breeding dispersal or alternative rescue dynamics, we included an estimable scaling parameter ($\kappa$). We evaluated model performance using simulation across different survival structures (constant, spatial, spatiotemporal), life histories, and CMR detection probabilities, and assessed robustness of inference when the occupancy-survival link is violated. We applied the model to long-term peregrine falcon (*Falco peregrinus*) data in Hungary, evaluating the effects on survival of the presence of a predator (eagle owl), and the proportion of agricultural land.

3. Survival estimated with the integrated model showed negligible bias and good coverage across all simulation scenarios, while substantially improving precision relative to CMR-only analyses. Precision gains were largest for spatial regression coefficients (up to 80%) and temporal variance parameters (up to 88%); they increased with model complexity and declining detection probability. When the occupancy-survival link was violated, $\kappa$ absorbed the resulting discrepancy and prevented bias in survival. In the case study, integration substantially improved the precision of spatiotemporal survival estimates and revealed a negative association with eagle owl presence and a positive one with the proportion of agricultural land.
4. Our new integrated model improves estimation of spatial and temporal variation in survival by leveraging shared information across data sources, extending spatially explicit demographic inference to systems where CMR data alone are insufficient, and thereby allowing spatial survival inference in a broader range of populations.

**Keywords:** survival estimation, integrated model, capture-mark-recapture, occupancy data, dynamic occupancy model, territorial species, spatial demography, peregrine falcon

## Introduction

Estimation of survival probability is a central objective in population ecology. Assessing variation of survival over time and space is essential for a sound understanding of population dynamics and for making informed management decisions (Koons et al., 2016; Morrison et al., 2022). By far the most common mode of survival estimation relies on capture-mark-recapture (CMR) studies, which consist of tagging and repeatedly encountering individuals over their lifetimes (Seber & Schofield, 2019). While the resulting data provide a solid basis for inference about survival, collecting them is costly logistically and economically (Lahoz-Monfort et al., 2014). As a result, CMR data are frequently limited in sample size and in their spatial and/or temporal scales (Lahoz-Monfort et al., 2014; Lees et al., 2021).

These constraints are especially restrictive when the interest extends beyond average survival to its heterogeneity in space. Spatial variation in survival reflects important ecological processes, such as habitat-specific survival and source-sink dynamics, or indicate areas of elevated mortality (Hernández-Matías et al., 2013; Furrer & Pasinelli, 2016). Identifying such patterns is often central to conservation planning, especially for prioritizing areas for management (Falcucci et al., 2009; González-Suárez et al., 2018). However, spatially-explicit models that assess variation of demographic parameters over space require substantially more data than their non-spatial counterparts. In CMR models, this typically requires large numbers of marked individuals that are monitored over time and over

as large spatial extents as possible (Péron et al., 2011; Saracco et al., 2012; Eacker et al., 2022; Schirmer et al., 2023; Milleret et al., 2025). In many systems, these requirements are difficult or even impossible to meet. Consequently, spatially explicit survival models remain very rare, and empirical evidence on spatial survival variation is still very limited for most species, despite its recognized ecological and conservation relevance (but see Saracco et al., 2010; Péron et al., 2011; Milleret et al., 2022).

In contrast to CMR data, biodiversity monitoring programmes that do not involve the tagging of any individuals may produce large datasets on presence/absence or population counts of species over large spatial domains (Brlík et al., 2021). A typical example is site occupancy data, which record whether discrete spatial units, or "sites", are occupied or not by some species during repeated survey occasions (MacKenzie et al. 2002). Such data are quite common for territorial species, which breed at well-defined sites occupied by a single individual or pair, such as nests, burrows, nestboxes, cliffs, or cavities (Sergio & Newton, 2003). For them, the occupancy status of a site (occupied or empty) is directly related to the local abundance at the site (one or zero breeding individual or pair), so that changes in occupancy patterns reflect changes in breeder population size (Kéry & Royle, 2021). Compared to capture-mark-recapture, occupancy data do not need individual recognition of animals, are far easier and less expensive to collect, enabling broader spatial coverage and longer time series. Moreover, occupancy data are naturally spatially explicit, making them convenient for studying spatial heterogeneity (MacKenzie et al., 2018).

Dynamic occupancy models provide a powerful analytical framework for analyzing territory occupancy (TO) data at discrete time steps (MacKenzie et al., 2003; Royle & Kéry, 2007).

These models have been widely applied to study changing species distributions and range dynamics, responses to environmental covariates, and they naturally accommodate spatial structure and site-level heterogeneity (MacKenzie et al., 2018). The dynamic occupancy model explicitly links the latent occupancy state of a site at a given time point to its state at the previous time point through a first-order Markov process. This temporal dependence is governed by persistence, i.e., the probability that an occupied site remains occupied, and colonization, which is the probability that an unoccupied site becomes occupied.

A key feature of the persistence parameter is that it is ultimately determined by individual-level demographic processes – a link initially recognized by Roth & Amrhein (2010). When occupancy of a site corresponds to the presence of a single individual or breeding pair, site persistence from one occasion to the next arises through one of two mutually exclusive mechanisms: i) survival and site fidelity of the current territory holder/s, or ii) loss of the holder/s through mortality or dispersal, followed by replacement through a new occupant. However, because individuals are not uniquely identified in TO data, survival cannot be distinguished from the other processes that drive occupancy dynamics without strong assumptions or additional information (Roth & Amrhein, 2010; Hernández-Matías et al., 2011; Oppel et al., 2016).

Interestingly, the strengths and limitations of CMR and TO data are complementary. CMR data provide direct information about survival but are often limited in spatial extent. TO data are often spatially richer but can inform survival only indirectly. Existing analytical approaches typically exploit one data source alone, but not both together: CMR models have a purely demographic focus but often lack spatial resolution, whereas occupancy models

are inherently spatially structured, but provide only limited demographic information. It is therefore desirable to combine CMR and TO data in a single model to leverage the strengths of both and mitigate the weaknesses in each.

Here, we develop an integrated model that combines CMR and TO data (Kéry & Royle 2021). Extending the model of Roth & Amrhein (2010), we describe the site-level occupancy process as a function of individual-level survival probabilities, allowing us to leverage information from both data sources to improve estimates of survival and assess its spatiotemporal variation. We first present three proofs of concept of the new model; initially for a situation where survival is constant over space and time. Then, we extend the model to estimate spatially varying survival, and finally to a scenario where both spatial and temporal survival variation is present. Using simulated data, we test the performance of all three models by comparing their estimates to data-generating values and to estimates of CMR-only models, to assess the precision gains resulting from the integration of the TO data. We further evaluate the estimates under these models for different life histories (long-lived, short-lived) and for low vs. high recapture probabilities to test model performance when CMR data are scarce. To assess the robustness of the integrated model, we also examine situations in which occupancy patterns are influenced by additional processes other than individual survival (e.g., breeding dispersal, altered rescue dynamics). Finally, we apply the integrated model to long-term monitoring data of a territorial raptor, the peregrine falcon *Falco peregrinus*, to explore the spatial effects of ecological predictors on survival. We expect our model to be particularly powerful for the study of spatial population dynamics,

enabling the assessment of spatial variation in survival and testing for factors that drive this variation.

**Methods**

We developed an integrated model that combines capture-mark-recapture (CMR) and territory occupancy (TO) data within a joint likelihood, thereby linking individual-level survival and site-level occupancy dynamics. The model is formulated hierarchically, with separate processes for individual survival and site occupancy that are linked through a shared survival component for breeders. Occupancy data are assumed to be collected across a set of breeding territories monitored over several years. CMR data originate from individuals marked and observed breeding from at least some of these territories.

Modelling site-level occupancy dynamics

Let ***z*** denote the occupancy data matrix that describes, for every site $s$, whether it is occupied ($z_{s,t} = 1$) or empty ($z_{s,t} = 0$) at occasion *t*. The state process in the first occasion $t = 1$ at site *s*, $z_{s,1}$, is modelled as a draw from a Bernoulli distribution with a probability $\psi$ (Equation 1).

$$z_{s,1} \sim Bernoulli(\psi)$$

*Equation 1*

From $t = 2$ onward, we model the occupancy state $z_{s,t}$ of site *s* at time *t* as a function of its state at time *t-1* through a first-order Markov process. This temporal dependence is governed by two parameters: persistence ($\phi$), i.e., the probability that a site occupied at occasion *t-1* remains occupied at time *t*, and colonization ($\gamma$), which is the probability that an unoccupied site at occasion *t-1* becomes occupied at occasion *t* (Equation 2). For convenience, we

express persistence and colonization as time-varying ($\phi_t$, $\gamma_t$), but they could also be expressed as time-constant.

$$z_{s,t} \sim Bernoulli\left(z_{s,t-1} \cdot \phi_t + \left(1 - z_{s,t-1}\right) \cdot \gamma_t\right)$$

*Equation 2*

Note that, for simplicity, we assumed perfect detection in the occupancy model, but imperfect detection could be accommodated in the usual way if detection/nondetection data from repeated within-season visits are available (Royle & Kéry, 2007).

To link the occupancy model with the individual-level survival process that underlies occupancy dynamics, we express persistence ($\phi$) as a function of individual survival of the territory holder ($S_B$) as well as colonization probability ($\gamma$). When a site is occupied at *t-1*, it remains occupied at *t* when either (i) the current breeder survives, or (ii) it dies, and is immediately replaced by another individual within the same interval (i.e., a "rescue effect", Roth & Amrhein, 2010). These are mutually exclusive events, and hence the probability of persistence at time *t* ($\phi_t$) is the following sum (Equation 3):

$$\phi_t = S_B + (1 - S_B) \cdot \gamma_t$$

*Equation 3*

<u>Biological assumptions of the model</u>

The model described above represents the theoretical demographic relationship expected between site persistence, colonization, and breeder survival. Importantly, it relies on three biological assumptions about territory occupancy dynamics and the breeding system. First,

each site can host at most one breeding female (or breeding pair in monogamous species), such that sites represent discrete breeding territories. Second, females exhibit complete site fidelity to their breeding site once recruited, implying that breeding dispersal does not occur in the baseline formulation of the model. Consequently, site turnover can arise only through mortality of the breeding female or site colonization by a new female breeder, but not by breeding dispersal. Third, the replacement of just-vacated or "rescued" sites occurs at the same rate as the colonization of sites that have been empty for one time step or longer (Equations 2-3). This assumption is needed because rescue events are typically unobserved and must therefore be inferred from overall colonization dynamics (Roth & Amrhein, 2010).

In the next section we address cases where these assumptions are violated.

Potential mismatch between persistence and its demographic decomposition

In practice, we expect that two of the above assumptions are not infrequently violated. First, breeding dispersal could occur and generate additional site turnover unrelated to mortality. This would lead to a reduction of site persistence while breeder survival remains the same (Roth & Amrhein, 2010).

Second, alternative rescue dynamics can produce the opposite discrepancy. For instance, if recently vacated sites are more likely to be filled, turnover events may remain undetected at the site level. This inflates observed persistence relative to survival. This phenomenon may be caused by conspecific attraction, whereby the presence of a remaining breeder of the former pair or conspecific cues may increase the probability that a site is rapidly

recolonized (Tapia & Zuberogoitia, 2018). This phenomenon is observed in several raptors (Hernández-Matías et al., 2011; Oppel et al., 2016).

Importantly, if site-level dynamics are influenced by these or other mechanisms and they are not represented in the persistence formulation (Equation 3), the strict deterministic link between persistence and breeder survival may induce bias, as the model attempts to reconcile mismatched occupancy patterns by adjusting survival estimates. This motivates the inclusion in our model of a scaling parameter to allow persistence to deviate from its deterministic demographic decomposition.

Relaxing the persistence-survival relationship by introducing a scaling parameter, "$\kappa$"

We introduce a scaling parameter, $\kappa$, that adds flexibility to the link between persistence and its demographic decomposition:

$$z_{s,t} \sim Bernoulli\left(z_{s,t-1} \cdot (S_B + (1 - S_B) \cdot \gamma_t) \cdot \kappa + \left(1 - z_{s,t-1}\right) \cdot \gamma_t\right)$$

*Equation 4*

When the relationship between persistence and individual survival holds exactly, $\kappa$ will be equal to 1. Values of $\kappa > 1$ indicate that persistence is greater than predicted from its demographic decomposition, whereas values of $\kappa < 1$ indicate that it is lower. Importantly, $\kappa$ does not distinguish among the biological mechanisms that may alter the persistence-demography relationship, nor is it intended to estimate their strength directly. Rather, it prevents bias in survival when site-level persistence reflects such additional processes.

Note that, to ensure that persistence remains within the (0,1) range, $\kappa$ and the persistence decomposition (Equation 2) are introduced in their corresponding link scales (see Equation S1).

Capture-mark-recapture submodel to estimate individual survival

For the CMR data we specified a Cormack-Jolly-Seber (CJS) model in the simulations and a multistate CMR model in the case study (Schaub & Kéry, 2022). To improve computational efficiency, we implemented the CJS and multistate models using a marginalized state-space likelihood that integrates over latent states while preserving individual identification (Schaub & Badia-Boher, 2025).

In all CMR models, we stratified survival and detection probabilities by age class, with the number of age classes depending on the life cycle of the modelled species (see "Simulations"). We assumed that all individuals become breeders at a fixed age which will vary according to the species life cycle. For simplicity, we modelled survival of all pre-breeder age classes as constant over time and space. In all cases, breeder survival $S_B$ was the only survival parameter in the CMR submodel that was linked to occupancy dynamics.

Extending the model to estimate variable survival across space

The model so far described assumes spatially homogeneous breeder survival. We now introduce a spatially explicit model by allowing breeder survival to vary between sites. The key to integrating TO and CMR data at the spatial level is to assign each individual in the CMR dataset to a specific breeding territory. Let $\delta$ be a categorical variable such that $\delta_i = 1 \ldots M$ denotes the breeding site of individual *i*, where *M* is the total number of territories in the

occupancy dataset. This ensures a one-to-one mapping between individuals and spatial units across the two submodels (Figure 1). Consequently, any site-level state or covariate in the occupancy model will be linked to the corresponding individual-level survival estimated in the CMR model. For individuals observed breeding at least once, $\delta_i$ is known, whereas for individuals that are never observed breeding, $\delta_i$ is missing and is therefore treated as a latent variable that is randomly drawn from the set of all sites in the occupancy dataset using a discrete uniform distribution.

Breeder survival can now be modelled as a function of site-level covariates:

$$logit(S_{B_s}) = \alpha + \beta \cdot x_s,$$

*Equation 5*

where $x_s$ is the value of a covariate at site $s$, $\alpha$ is the intercept, and $\beta$ is the coefficient quantifying how survival changes with $x$.

To propagate the information on spatial variation in breeder survival to the individual-level CMR likelihood, we assign each individual in the CMR dataset the survival probability associated with its breeding site $\delta_i$. Specifically, for each individual $i$, individual-level breeder survival $S'_{B_i}$ is:

$$S'_{B_i} = S_{B_{\delta_i}}$$

*Equation 6*

For instance, if individual $i = 1$ is recorded as a breeder at site $s = 10$, then $\delta_1 = 10$, and therefore it is assigned the breeder survival probability $S_B$ of site 10.

$$S'_{B_1} = S_{B_{\delta_1}} \rightarrow S'_{B_1} = S_{B_{10}}$$

*Equation 7*

This mapping ensures that the same site-specific breeder survival parameter applies both for the individual survival process in the CMR submodel and the site persistence process in the dynamic occupancy submodel.

Site persistence is expressed as a function of breeder survival and colonization probabilities as described previously, but now incorporating a site dimension $s$.

$$\phi_{s,t} = S_{B_s} + \left(1 - S_{B_s}\right) \cdot \gamma_t,$$

*Equation 8*

The state process of the joint likelihood is modified accordingly, while the remaining components stay the same:

$$z_{s,t} \sim Bernoulli\left(z_{s,t-1} \cdot \left(S_{B_s} + \left(1 - S_{B_s}\right) \cdot \gamma_t\right) \cdot \kappa + \left(1 - z_{s,t-1}\right) \cdot \gamma_t\right)$$

*Equation 9*

Modelling temporal variation alongside spatial variation is a natural extension. For instance, we may add unstructured temporal random effects for breeder survival.

$$logit\left(S_{B_{s,t}}\right) = \alpha + \beta \cdot x_s + \epsilon_t;\ \epsilon_t \sim Normal(0, \sigma)$$

*Equation 10*

Evaluation of model performance using simulations

We conducted two simulation studies. In the first, we evaluated the performance of the integrated model just described in terms of accuracy and precision across a range of modelling and biological scenarios. In the second, we assessed the role of the scaling

parameter $\kappa$ in ensuring unbiased survival inference when the assumed strict demographic link between breeder survival and site persistence is violated.

Simulation study 1: bias, coverage, and precision gains of the integrated model under different survival structures

Simulations varied along three dimensions: (i) survival from simple to more complex (constant, spatial only, spatiotemporal), (ii) life history (short- vs. long-lived species), and (iii) detection probability in the CMR data (low *vs.* high). For each scenario, we also compared inferences from the integrated model with those from a CMR-only model to assess the gains in precision resulting from the integrated model. We simulated 500 datasets per scenario, totalling 6,000 simulated datasets (500 datasets x 3 survival structures x 2 life cycles x 2 recapture effort scenarios) and 12,000 fitted models (an integrated and a CMR model for each dataset).

Description of simulations

We simulated data under an individual-based, space-structured population model with a fixed number of breeding sites, each of which could hold at most one breeding female, and with discrete annual time steps. We modelled site persistence directly from breeder survival and colonization according to the demographic decomposition in Equation 3. Under these simulation conditions, no mismatch occurs, and hence $\kappa$ is equal to 1 by definition. For each year, we sequentially simulated, survival/mortality, aging, assignment to a breeding site of each individual reaching the age of first breeding, and productivity (for further details see Appendix S1).

Comparison with CMR-only models

To evaluate gains in accuracy and precision obtained through data integration, we fitted CJS models to each simulated CMR dataset. Namely, for (i) the model with constant survival, we fitted a nonspatial CJS. Likewise, for (ii) the spatial model and (iii) the spatiotemporal model, we compared the results to CJS models estimating spatially-varying survival and spatiotemporally-varying survival respectively. See Appendix S1 for further details.

We evaluated the frequentist operating characteristics of estimates from both models by computing relative bias (accuracy), mean length of the 95% posterior credible intervals (precision) and coverage of 95% credible intervals.

Simulation study 2: The role of the scaling parameter $\kappa$ in ensuring unbiased survival estimates

Here, we assessed whether the inclusion of the scaling parameter $\kappa$ results in unbiased estimates of survival when key assumptions of the integrated model are violated. We included two processes in the data generation that break the assumed relationship between breeder survival and site persistence: breeding dispersal and altered rescue dynamics. Because breeding dispersal is expected to reduce persistence relative to its demographic decomposition, it induces values of $\kappa < 1$. Conversely, alternative rescue dynamics – in which recently vacated sites are recolonized more rapidly than sites that were empty for longer – are expected to increase persistence relative to its deterministic decomposition, and hence induce values of $\kappa > 1$.

We generated three sets of 500 simulated datasets: i) with breeding dispersal, ii) with altered rescue dynamics, and iii) with both processes altogether. We then fitted two models to the resulting simulated datasets: (a) the integrated model including the scaling parameter $\kappa$, and (b) an equivalent model where $\kappa$ was removed from the joint likelihood. Comparing survival estimates between the two model formulations illustrates the role of $\kappa$ in ensuring unbiased estimates of survival and illustrates potential biases in breeder survival in its absence. See Appendix S1 for further details.

Statistical inference and model fitting

We fitted all models using Bayesian MCMC in package Nimble (de Valpine et al., 2017) run from R version 4.5.2 (R Core Team, 2024). In each analysis, we ran four chains of 20,000 iterations with the first 10,000 discarded as burn-in and the remainder thinned by 1 in 20. Convergence was confirmed visually using traceplots and by values of the Brooks-Gelman-Rubin statistic Rhat<1.06.

We specified vague priors for most parameters. Parameters defined on the probability scale (intercepts of survival and detection, and first-year occupancy probability) were assigned Beta(1,1) priors. Regression coefficients were assigned Gaussian priors with mean 0 and standard deviation 4. For random-effects standard deviations, we used weakly informative half-Cauchy priors with scale parameter 1 (Gelman, 2006), which provide mild regularization, while allowing for substantial temporal variation in survival probabilities. Kappa was modelled with a log-link and assigned a uniform prior from 0 to 5.

Case study: Spatial patterns in the survival of Hungarian peregrine falcons

We applied the new integrated model to long-term monitoring data from an expanding peregrine falcon population in Hungary over 27 years (1997-2023; Prommer et al., 2026a, 2026b). Monitoring data included (i) yearly assessments of the occupancy status of up to 146 breeding territories; and (ii) resighting and dead recovery data for 893 birds ringed as fledglings, of which 104 were ever resighted, 61 were resighted as breeders, and 23 were recovered dead (further details in Appendix S1).

We fitted the integrated model to the combined CMR and occupancy data and, for comparison, we also fitted a CMR model to the CMR data alone. CMR and recovery data in both models were analyzed using a multistate capture-mark-recapture-recovery likelihood implemented via a marginalized state-space likelihood (Burnham, 1993; Schaub & Badia-Boher, 2025). We assumed individuals became breeders at the age of two years (Prommer et al., 2026a), and modelled breeder survival as varying spatially according to two site-level covariates, one discrete and the other continuous, and also included an unstructured random effect of the year. Full model specifications are shown in Appendix S1.

As a first, discrete site-level covariate, we used the presence of Eurasian eagle owl (*Bubo bubo)* breeding territories within a 2 km radius of peregrine breeding sites at any time during 1997–2023. The potential effect of eagle-owls on peregrine falcon population dynamics is receiving increased attention in raptor studies (Kéry et al., 2025; Prommer et al., 2026a; Prommer et al., 2026b). Eagle-owl predation and competition is suspected to be a main contributor for current declines of some peregrine falcon populations across Europe (e.g., Kéry et al., 2022, 2025). In the Hungarian study population, the eagle owl is suspected to cause regional declines in peregrine falcon productivity in areas where the range of both

species overlap (Prommer et al., 2026b). Furthermore, there have been increasing reports of predation of young and adult peregrine falcons by eagle owls (unpublished data). Nevertheless, to date no studies have provided direct estimates of eagle owl effects on peregrine survival.

As a second, continuous site-level covariate, we included the year-specific proportion of agricultural land within each peregrine falcon territory (i.e., within a 4 km buffer around the nest; Prommer et al., 2026b). Open agricultural areas may enhance survival by favouring the peregrine's mid-air hunting mode and increasing availability of key prey like pigeons, relative to forested habitats (Ratcliffe, 1993). However, they may also decrease survival due to higher densities of power lines and pylons, increasing electrocution and collision risks. We therefore tested for the presence of any positive or negative association between agricultural land and survival.

**Results**

Simulation study 1: bias, coverage, and precision gains of the integrated model under different survival structures

The integrated model accurately recovered data-generating values across survival structures, life histories, and detection probabilities (Figure 2; Tables S1, S2, S3). Coverage of estimates of survival parameters (mean survival in constant scenarios, survival intercepts in spatial models, and survival hypermeans in spatiotemporal models) was at the nominal level around 95%. The relative bias for these parameters was low to negligible (<2%). The

largest, but still mild, bias (< 5%) occurred in the spatiotemporal model fitted to short-lived species under low detection.

Estimates of spatial regression coefficients ($\beta$) showed negligible bias across all spatial and spatiotemporal scenarios, and coverage was slightly below the nominal level (89-95%; Tables S2, S3). In the spatiotemporal scenario, temporal variance estimates showed a small positive bias (3-13%), but this was also present in CMR-only models, and coverage was good across scenarios (94-97%; Table S3). Year-specific survival estimates in spatiotemporal models showed negligible bias (<1.2%) across most scenarios, with slightly larger bias (3.8%) under low detection in short-lived species (Table S3).

In this simulation study, $\kappa$ was 1 by definition, since we modelled no disagreement between persistence and its demographic decomposition. Using this value as a reference, $\kappa$ achieved coverage over 95% across scenarios, and bias from 1 was low under high detection (0-4%) and modest under low detection (1-7%). Colonization probability $\gamma$ also achieved coverage over 95% and negligible bias (Tables S1, S2, S3).

We quantified precision gains as the proportional reduction in credible interval length of integrated models, relative to that from CMR-only models (Figure 3, Table S4). In models with constant survival, gains were modest (0-4%), particularly under high detection. In spatial models, however, gains became more pronounced, reaching, under high and low detection scenarios respectively, 5-12% for the survival intercept and 49-73% for the spatial regression coefficient. The largest gains occurred in spatiotemporal models: precision increased by 21% and 38% for high and low detection scenarios respectively for the survival hypermean,

55% and 80% for the spatial regression coefficient, 47% and 88% for the temporal variance parameter, and 31% and 46% for yearly survival estimates. Across most parameters, precision gains were slightly greater for short-lived species, especially when detection was low.

Simulation study 2: The role of the scaling parameter $\kappa$ in ensuring unbiased survival estimates

Under all three mismatch scenarios (breeding dispersal, altered rescue dynamics, and both processes combined), models excluding $\kappa$ produced survival estimates whose bias increased approximately linearly with the magnitude of the violation (Figure 4). Including $\kappa$ substantially reduced this bias across all scenarios (Figure 4). Estimates of $\kappa$ declined progressively with increasing dispersal probability and increased progressively with the strength of the rescue effect, consistent with our expectations (Figure S1).

Case study: Spatial patterns in the survival of Hungarian peregrine falcons

The integrated model estimated mean breeder survival at 0.772 (95%CRI: 0.69, 0.85), very similar to the CMR-only estimate (0.779, 95%CRI: 0.65, 0.92), but 39% more precise (Figure S2). Annual survival estimates in the integrated model mostly ranged between 0.6 and 0.85. Relative to the CMR-only model, precision of annual estimates increased by ca. 50% in the early years of the study (1997-2008), when capture-mark-recapture samples were smallest, and by ca. 30% in later years when sample sizes were larger (Figure 5A).

There was a tendency for peregrine territories overlapping with eagle owl territories to have lower survival (-0.07, 95%CRI: -0.22, 0.07), with a 82% probability of a negative effect (Figure

5B). Further, we found moderate evidence of a positive association between the proportion of agricultural land within territories and survival ($\beta$ = 0.07, 95%CRI: -0.05, 0.19), with 86% probability of a positive effect (Figure 5C). Precision of the coefficients of the two spatial covariates in survival increased by 42% and 71%, respectively, in the integrated model relative to the CMR-only model (Figures 5C, S3). Overall, mean territory-specific survival probabilities ranged between 0.68 and 0.8 and reached lowest values in territories with eagle owl presence combined with low proportions of agricultural land (Figure 5D). The scaling parameter $\kappa$ was estimated as substantially greater than 1 (3.42, 95%CRI: 2.27, 4.96; Figure S4).

**Discussion**

We developed a new integrated model that combines territory occupancy (TO) and capture-mark-recapture (CMR) data by expressing persistence probabilities in the former as a function of individual-level survival. The model yielded substantially improved inferences on survival and its spatiotemporal variation, while preserving statistical accuracy. Across all simulated survival scenarios, life histories, and CMR detection scenarios, the integrated model maintained adequate coverage and low to negligible bias, while consistently increasing precision relative to CMR-only analyses. Precision gains increased with the complexity of the survival model and with declining detection probability. Parameters that are typically harder to estimate in a CMR-only framework – spatial regression coefficients and temporal variances – benefited most from the integration of the occupancy data, with precision gains of up to 80%. These results demonstrate that our model performs well across

a broad range of different scenarios and is particularly effective for estimating spatial variation in survival, one of the most 'elusive' parameters in the study of animal demography.

The gains in precision arise from the shared demographic information between both data sources. When survival varies across space and time, combined with low CMR detection probabilities, CMR data alone may provide only limited information about spatial and temporal variation in survival. By explicitly linking survival to territory-level occupancy dynamics, the integrated model draws additional information from site persistence patterns that partially reflect the underlying survival processes. This joint structure can therefore strengthen the estimates of spatial and temporal effects.

Compared to existing approaches that estimate spatial variation in survival, our new model differs in the following manners. Spatially explicit CMR models (Saracco et al., 2010; Péron et al., 2011; Milleret et al., 2022) can estimate survival variation across space and can accommodate spatial covariates, but the information to estimate survival in these settings is entirely derived from data of marked individuals (including genetic samples or natural markings). When recaptures are sparse or sample sizes small, estimates of spatial effects may become uncertain or inestimable. This restricts the application of these methods to large or very large datasets of marked individuals broadly distributed across space (e.g., Saracco et al., 2010, 2012; Milleret et al., 2025). Our approach relaxes this constraint by using additional information from occupancy data on unmarked individuals, which are naturally spatially disaggregated and typically more abundant. This substantially extends the capacity to estimate spatial patterns in survival to systems where marking data might be sparse, but TO data are available.

Our new model is an integrated model but differs from Integrated Population Models (IPMs; Schaub & Kéry, 2022) in both spatial resolution and focus. Most IPMs assume spatially constant survival (Schaub & Kéry, 2022) and the development of spatially explicit IPMs is still in its early stages (Chandler & Clark, 2014; Zhao et al., 2020, Ketwaroo et al., 2026). Interestingly, population counts used in IPMs often originate from territory occupancy data that are naturally spatially disaggregated, but are collapsed into population-wide totals at analysis (e.g., Fay et al., 2019; Martin et al., 2025; Badia-Boher et al., 2026). Our model retains the original spatial structure in the counts by directly using occupancy data, and hence, as opposed to typical IPMs, we utilize all the spatial information these data naturally contain. Another difference is that our model remains focused on survival rather than on estimating full population dynamics as IPMs do (Schaub & Kéry, 2022). However, our model could be a foundation for the development of a spatially explicit IPM based on TO, CMR, and productivity data.

Our model requires that occupancy information refers to the presence or absence of a single breeder or breeding pair at each site. If instead occupancy denotes the presence of more than two breeders or may include nonbreeding individuals, the assumed link between site persistence and individual survival will no longer hold. This restricts application to territorial systems with discrete, identifiable breeding sites, yet such systems span a broad range of taxa that are often intensively monitored (Maher & Dale, 2000), such as cliff- or tree-nesting raptors, territorial passerines, non-colonial birds using nestboxes or cavities, and territorial burrowing mammals and reptiles. In this respect, our simulations, which encompassed both short- and long-lived species, suggest that the model performs well across a range of life

histories, supporting its general applicability within territorial systems, even with low detection probabilities and small sample sizes.

The scaling parameter $\kappa$ plays a central role in ensuring the demographic link between individual survival and site persistence. Our simulations showed that including $\kappa$ effectively removes bias in survival probabilities when the assumed persistence decomposition is violated. Such violations are likely to be common in real data, where different unmodelled biological processes could affect the persistence-survival relationship. Indeed, in our case study with Hungarian peregrine falcons, $\kappa$ was estimated as substantially greater than 1. A plausible biological explanation is a strong rescue effect related to conspecific attraction (as discussed previously in the Methods), common in territorial raptors (Hernández-Matías et al., 2011; Tapia & Zuberogoitia, 2018). Such dynamics generate $\kappa > 1$, as also demonstrated in our simulations (Figure 4B). But even then, mean annual breeder survival was estimated as practically identical to that of CMR-only models, but more precise, and consistent with published estimates for other peregrine falcon populations (e.g., Smith et al., 2015; Kéry et al., 2025; Badia-Boher et al., 2026; Gould et al., 2026).

The case study also illustrates the practical value at estimating spatiotemporal variation in survival with real datasets when CMR sample sizes are limited. Consistent with our simulations, data integration substantially increased the precision for estimates of spatial coefficients, temporal variance, and annual survival relative to CMR-only models. We found inconclusive (82% posterior probability), but suggestive evidence of a negative association between eagle owl presence and peregrine falcon survival, consistent with field reports of eagle owl predation of adult peregrines and with documented effects on productivity (e.g.,

Prommer et al., 2026b). We also found moderate evidence (86% posterior probability) that a higher proportion of agricultural land within territories is associated with greater breeder survival, consistent with the species' tolerance of human-modified landscapes and potentially reflecting enhanced hunting opportunities relative to forested areas (Ratcliffe, 1993). Besides, the integrated model also enables the construction of territory-specific survival maps (Figure 4D), which may serve as practical tools for prioritizing conservation efforts at sites with elevated mortality risk.

Several extensions of our model could be envisioned. If detection/nondetection data from repeated visits within a breeding season are available, the probability to detect an occupied territory could be estimated by extending the model by an observation model in the usual way (MacKenzie et al. 2002). In this way one can relax the assumption that occupied sites are perfectly detected conditional on site visitation, which in practice may often not be the case. As another potential extension, incorporating productivity data would allow the development of fully spatially disaggregated IPMs that jointly estimate site-level fecundity rates and survival probabilities. Additional refinements could focus on modelling processes that are now subsumed in the parameter $\kappa$: explicitly modelling breeding dispersal, or – in systems where persistence depends on survival of both territory holders – modelling pair survival. A further extension would replace or complement the covariate-based approach to spatial variation used here with spatially structured random effects – for instance, conditional autoregressive (CAR) or Gaussian process structures over the site-level survival parameters (Saracco et al., 2012; Schaub & Kéry 2022; Ketwaroo et al., 2026). This would allow the model to estimate smooth spatial survival surfaces across the landscape even in

the absence of any measured covariates, which may be particularly valuable when the drivers of spatial variation are unknown.

In conclusion, our study shows how integrating individual-level capture-mark–recapture data with site-level territory occupancy data is possible and that it substantially improves estimates of survival and its spatiotemporal variation. By allowing site-level persistence dynamics to inform survival estimation, the framework reduces reliance on CMR data alone and extends spatial and temporal survival inference to systems where marked samples are limited but occupancy data are available. This broadens the range of demographic datasets from which temporal but especially spatial heterogeneity in survival can be reliably estimated, and likewise, the number of populations and species from which relevant spatial insights can be extracted for conservation. More broadly, we hope the framework will contribute to advancing population ecology in spatially structured systems and open new avenues for integrated analyses that retain the spatial structure inherent in territory occupancy data.

**Acknowledgements**

We thank members and supporters of the Hungarian Peregrine Falcon Conservation Working Group and the Eurasian Eagle Owl Conservation Group coordinated by Zoltán Petrovics, initiatives led by MME-Birdlife Hungary, for their commitment over more than two decades of monitoring. We are also grateful to other volunteers and institutions that supported data collection. We thank the members of the Population Biology Unit, Swiss

Ornithological Institute, for constructive scientific discussions. This research was funded by the Swiss National Science Foundation grant number 310030_207603.

**Conflict of interest statement**

The authors declare no conflict of interests.

**Author contributions**

Jaume A. Badia-Boher, Marc Kéry, and Michael Schaub conceived the main ideas of the study. Mátyás Prommer designed and performed field work, arranged the data and helped with discussions about the case study. Jaume A. Badia-Boher performed the statistical analyses with support from Marc Kéry and Michael Schaub and led the writing of the manuscript. All authors provided critical feedback during manuscript elaboration.

**References**

Badia-Boher, J.A., Schaub, M., Mollet, M., Van Geneijgen, P., Van Der Jeugd, H.P., Caliendo, V., & Kéry, M. (2026). Evaluating the demographic impacts of the highly pathogenic avian influenza panzootic. *Journal of Applied Ecology*, *63*(1), e70234.

Burnham, K.P. (1993). A theory for combined analysis of ring recovery and recapture data. In J.D. Lebreton & P.M. North (Eds.), *Marked individuals in the study of bird populations* (pp. 199-213). Birkhäuser Verlag.

Brlík, V., Šilarová, E., Škorpilová, J., Alonso, H., Anton, M., Aunins, A., ..., & Chodkiewicz, T. (2021). Long-term and large-scale multispecies dataset tracking population changes of common European breeding birds. Scientific Data, 8(1), 21.

Chandler, R.B., & Clark, J.D. (2014). Spatially explicit integrated population models. Methods in Ecology and Evolution, 5(12), 1351–1360.

de Valpine, P., Turek, D., Paciorek, C.J., Anderson-Bergman, C., Temple Lang, D., & Bodik, R. (2017). Programming with models: writing statistical algorithms for general model structures with NIMBLE. *Journal of Computational and Graphical Statistics*, 26, 403-413.

Eacker, D.R., Jakes, A.F., & Jones, P.F. (2023). Spatiotemporal risk factors predict landscape-scale survivorship for a northern ungulate. *Ecosphere*, *14*(2), e4341.

Falcucci, A., Ciucci, P., Maiorano, L., Gentile, L., & Boitani, L. (2009). Assessing habitat quality for conservation using an integrated occurrence-mortality model. Journal of Applied Ecology, 46(3), 600–609.

Fay, R., Michler, S., Laesser, J., & Schaub, M. (2019). Integrated population model reveals that kestrels breeding in nest boxes operate as a source population. Ecography, 42(12), 2122–2131.

Furrer, R.D., & Pasinelli, G. (2016). Empirical evidence for source–sink populations: A review on occurrence, assessments and implications. Biological Reviews, 91(3), 782–795.

Gelman, A. (2006). Prior distributions for variance parameters in hierarchical models (comment on article by Browne and Draper). *Bayesian Analysis*, 1(3), 515-533.

González-Suárez, M., Zanchetta Ferreira, F., & Grilo, C. (2018). Spatial and species-level predictions of road mortality risk using trait data. Global Ecology and Biogeography, 27(9), 1093–1105.

Gould, M.J., Swem, T., Zimmerman, G.S., Millsap, B.A., Gedir, J.V., & Abadi, F. (2026). Status assessment of peregrine falcons in North America using integrated population models. *Global Ecology and Conservation*, *65*, e04024.

Hernández-Matías, A., Real, J., & Pradel, R. (2011). Quick methods for evaluating survival of age-characterizable long-lived territorial birds. *The Journal of Wildlife Management*, *75*(4), 856–866.

Hernández-Matías, A., Real, J., Moleón, M., Palma, L., Sánchez-Zapata, J.A., Pradel, R., ..., & García, J. (2013). From local monitoring to a broad-scale viability assessment: A case study for the Bonelli's Eagle in western Europe. Ecological Monographs, 83(2), 239–261.

Kéry, M., & Royle, J.A. (2021). *AHM1 – Modeling distribution, abundance and species richness using R and BUGS. Volume 2: Dynamic and Advanced Models*. Academic Press.

Kéry, M., Banderet, G., Müller, C., Pinaud, D., Savioz, J., Schmid, H., Werner, S., & Monneret, R.J. (2022). Spatio-temporal variation in post-recovery dynamics in a large Peregrine Falcon (Falco Peregrinus) population in the Jura mountains 2000-2020. *Ibis*, 164, 217-239.

Kéry, M., Monneret, R.J., Badia-Boher, J.A., & Schaub, M. (2025). Demographic causes of the pesticide crash in the peregrine falcon. *Ecoevorxiv*, *https://doi.org/10.32942/X2R05B*

Ketwaroo, F.R., Muller, M.H., Saracco, J.F., & Schaub, M. (2026). *An Integrated Population Model to Incorporate Spatio-Temporal Heterogeneity in Demographic Rates*. *BioRxiv*. https://doi.org/10.64898/2026.03.03.709263

Koons, D.N., Iles, D.T., Schaub, M., & Caswell, H. (2016). A life-history perspective on the demographic drivers of structured population dynamics in changing environments. *Ecology Letters,* 19(9), 1023–1031.

Lahoz-Monfort, J.J., Harris, M.P., Morgan, B.J.T., Freeman, S.N., & Wanless, S. (2014). Exploring the consequences of reducing survey effort for detecting individual and temporal variability in survival. *Journal of Applied Ecology,* 51(2), 534–543.

Lees, K.J., MacNeil, M.A., Hedges, K.J., & Hussey, N.E. (2021). Estimating demographic parameters for fisheries management using acoustic telemetry. *Reviews in Fish Biology and Fisheries*, 31(1), 25–51.

MacKenzie, D.I., Nichols, J.D., Lachman, G.B., Droege, S., Royle, J.A., & Langtimm, C.A. (2002). Estimating site occupancy rates when detection probabilities are less than one. *Ecology*, 83(8), 2248-2255.

MacKenzie, D.I., Nichols, J.D., Hines, J.E., Knutson, M.G., & Franklin, A.B. (2003). Estimating site occupancy, colonization, and local extinction when a species is detected imperfectly. Ecology, 84(8), 2200–2207.

MacKenzie, D.I., Nichols, J.D., Royle, J.A., Pollock, K.H., Bailey, L.L., & Hines, J.E. (2018). *Occupancy estimation and modelling. Inferring patterns and dynamics of species occurrence. Second Edition*. Academic Press.

Maher, C.R., & Lott, D.F. (2000). A review of ecological determinants of territoriality within vertebrate species. *The American Midland Naturalist*, 143(1), 1–29.

Martin, E.C., Riecke, T.V., Ravussin, P., Arrigo, D., & Schaub, M. (2026). Identifying the demographic pathways linking environmental covariates to population dynamics in an avian migrant. Ecological Applications, 36(1), e70166.

Milleret, C., Dey, S., Dupont, P., Brøseth, H., Turek, D., De Valpine, P., & Bischof, R. (2023). Estimating spatially variable and density-dependent survival using open-population spatial capture–recapture models. *Ecology*, *104*(2), e3934.

Milleret, C., Dupont, P., Dey, S., Brøseth, H., Kindberg, J., Turek, D., de Valpine, P., Åkesson, M., Wabakken, P., & Zimmermann, B. (2025). Map of death: Spatially explicit mortality of the grey wolf. *Proceedings of the Royal Society B: Biological Sciences*, *292*(2053).

Morrison, C.A., Butler, S.J., Clark, J.A., Arizaga, J., Baltà, O., Cepák, J, ..., & Gill, J.A. (2022). Demographic variation in space and time: Implications for conservation targeting. *Royal Society Open Science*, *9*(3), 211671.

Oppel, S., Dobrev, V., Arkumarev, V., Saravia, V., Bounas, A., Kret, E., ..., & Nikolov, S.C. (2016). Assessing the effectiveness of intensive conservation actions: Does guarding and feeding increase productivity and survival of Egyptian Vultures in the Balkans? *Biological Conservation*, *198*, 157–164.

Péron, G., Ferrand, Y., Gossmann, F., Bastat, C., Guenezan, M., & Gimenez, O. (2011). Nonparametric spatial regression of survival probability: Visualization of population sinks in Eurasian Woodcock. *Ecology*, *92*(8), 1672–1679.

Prommer, M., Badia-Boher, J.A., Kéry, M., Schaub, M., Bagyura, J., & Oli, M.K. (2026a). Evaluating population resilience to anticipated stressors using integrated population

modelling: a case study of Peregrine Falcons. *EcoEvoRxiv*, https://doi.org/10.32942/X2BH31.

Prommer, M., Bagyura, J., Kéry, M., & Oli, M.K. (2026b). Repopulation of the former breeding range: Spatio-temporal patterns and drivers of reproduction in the Peregrine Falcon (*Falco peregrinus* ) population in Hungary. *Ibis*, *168*(1), 63–78.

R Core Team (2024). R: A Language and Environment for Statistical Computing. *R Foundation for Statistical Computing*.

Ratcliffe, D. A. (1993). *The peregrine falcon*. T & AD Poyser.

Roth, T., & Amrhein, V. (2010). Estimating individual survival using territory occupancy data on unmarked animals. *Journal of Applied Ecology*, *47*(2), 386–392.

Royle, J.A., & Kéry, M. (2007). A Bayesian state-space formulation of dynamic occupancy models. Ecology, 88(7), 1813–1823.

Saracco, J.F., Royle, J.A., DeSante, D.F., & Gardner, B. (2010). Modeling spatial variation in avian survival and residency probabilities. *Ecology*, *91*(7), 1885–1891.

Saracco, J.F., Royle, J.A., DeSante, D.F., & Gardner, B. (2012). Spatial modeling of survival and residency and application to the Monitoring Avian Productivity and Survivorship program. *Journal of Ornithology*, *152*(S2), 469–476.

Schaub, M., & Badia-Boher, J.A. (2025). Comparison of Bayesian Models to Estimate Survival From Dead-Recovery Alone and Together With Live-Encounter Data: Challenges and Opportunities. *Ecology and Evolution*, *15*(6), e71517.

Schaub, M., & Kéry, M. (2022). *Integrated population models: Theory and ecological applications with R and JAGS*. Academic Press.

Schirmer, S., Korner-Nievergelt, F., Von Rönn, J.A.C., & Liebscher, V. (2023). Estimating survival in continuous space from mark-dead-recovery data—Towards a continuous version of the multinomial dead recovery model. *Journal of Theoretical Biology*, *574*, 111625.

Seber, G.A.F., & Schofield, M.R. (2019). *Capture-Recapture: Parameter Estimation for Open Animal Populations*. Springer.

Sergio, F., & Newton, I. (2003). Occupancy as a measure of territory quality. Journal of Animal Ecology, 72(5), 857–865.

Smith, G.D., Murillo-García, O.E., Hostetler, J.A., Mearns, R., Rollie, C., Newton, I., McGrady, M.J., & Oli, M.K. (2015). Demography of population recovery: Survival and fidelity of Peregrine Falcons at various stages of population recovery. *Oecologia*, *178*(2), 391–401.

Tapia, L., & Zuberogoitia, I. (2018). Breeding and Nesting Biology in Raptors. In J.H. Sarasola, J.M. Grande, & J.J. Negro (Eds.), *Birds of Prey: Biology and conservation in the XXI century* (pp. 63–94). Springer International Publishing.

Zhao, Q. (2020). On the sampling design of spatially explicit integrated population models. Methods in Ecology and Evolution, 11(10), 1207–1220.

**Figure legends**

Figure 1. Example structure of the site-occupancy (left) and capture-mark-recapture (right) datasets used in the integrated analysis. For illustration, we use a hypothetical "short-lived" species for which all individuals become breeders at age 1. Each individual *i* in the capture-mark-recapture dataset is associated with a breeding site $\delta_i$, linking individual encounter histories to the corresponding site in the occupancy dataset. Bold blue entries illustrate observations contributing shared information across the two data sources. Column names "y-" indicate years.

Figure 2. Relative bias (%) of survival parameters across simulated survival scenarios (constant, spatial, spatiotemporal), life histories ("Long-L" and "Short-L" for long-lived and short-lived species respectively), and capture-mark-recapture detection efforts ("Low-P" and "High-P" for low and high detection efforts, respectively). Colors indicate survival scenarios. Boxplots summarize results across simulations per scenario and depict median bias (central line), interquartile range (IQR, box) and whiskers extending to the most extreme observations within 1.5 x IQR; outliers are not shown.

Figure 3. Mean credible interval (CRI) length, i.e., precision, for survival parameters across simulated survival scenarios (constant, spatial, spatiotemporal), life histories ("Long-L" for long-lived species and "Short-L" for short-lived species), and capture-mark-recapture detection efforts ("Low-P" and "High-P" for low and high detection efforts, respectively). For each simulation scenario, the results of capture-mark-recapture-only and integrated models are compared. Points show mean CRI lengths, and vertical lines denote $2.5^{th}$ and $97.5^{th}$ percentiles of CRI lengths.

Figure 4. Relative bias (%) in breeder survival estimates $S_B$ under increasing mismatch between persistence and its demographic decomposition: (A) Relative bias as a function of breeding dispersal probability; (B) Relative bias as a function of rescue effect strength; (C) Combined effects of breeding dispersal and rescue dynamics on the relative bias. The coloured surface in (C) shows a smoothed relative bias surface estimated using a generalized additive model, with points indicating simulation-specific $S_B$ estimates. Facets indicate models including $\kappa$ ("KAPPA") and excluding $\kappa$ ("NO").

Figure 5. Results of the case study with Hungarian peregrines. (A) Annual breeder survival probabilities estimated by the integrated and the capture-mark-recapture-only model. Lines represent posterior means and shaded areas 95% credible intervals. (B) Posterior distributions of mean breeder survival probability under presence versus absence of eagle owl territories. (C) Estimated relationship between breeder survival probability and the proportion of agricultural land surrounding territories in integrated and capture-mark-recapture-only models. (D) Mean breeder survival probabilities across breeding territories in Hungary; coordinates are displayed as geographic longitude (X) and latitude (Y) in decimal degrees (WGS84).

## Figures

### Figure 1

Site occupancy data

| site | y1 | y2 | y3 | y4 | y5 |
|---|---|---|---|---|---|
| 1 | 1 | **1** | 0 | 1 | 1 |
| 2 | 0 | 0 | 0 | 1 | 0 |
| 3 | 1 | 1 | **1** | **1** | **1** |
| 4 | 0 | 0 | 0 | 0 | 0 |
| 5 | 0 | 0 | 1 | 1 | 1 |
| 6 | 0 | 0 | 1 | 0 | 0 |
| 7 | 0 | 0 | 0 | 1 | **1** |
| 8 | 0 | **1** | **1** | **1** | **1** |
| 9 | 0 | 0 | 0 | 0 | 1 |

Capture–recapture data

| individual | $\delta_i$ | y1 | y2 | y3 | y4 | y5 |
|---|---|---|---|---|---|---|
| 1 | 1 | 1 | **1** | 0 | 0 | 0 |
| 2 | 3 | 0 | 1 | **1** | **1** | 0 |
| 3 | 3 | 0 | 0 | 0 | 1 | **1** |
| 4 | 7 | 0 | 0 | 0 | 1 | **1** |
| 5 | 8 | 1 | **1** | **1** | **1** | **1** |

**Figure 2**

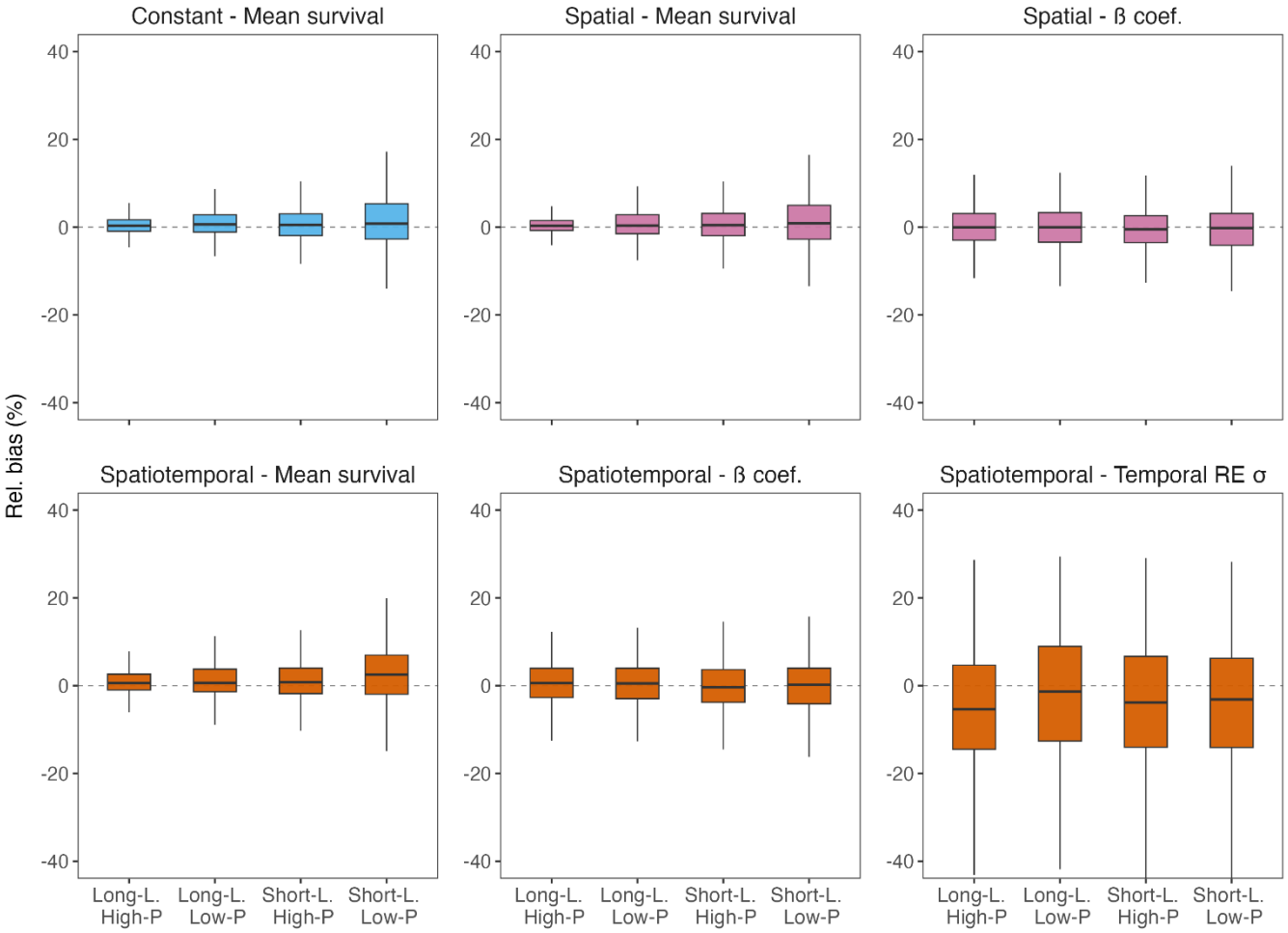
Constant - Mean survival
Spatial - Mean survival
Spatial - ß coef.
Spatiotemporal - Mean survival
Spatiotemporal - ß coef.
Spatiotemporal - Temporal RE σ
Rel. bias (%)
40
20
0
-20
-40
Long-L. High-P
Long-L. Low-P
Short-L. High-P
Short-L. Low-P

**Figure 3**

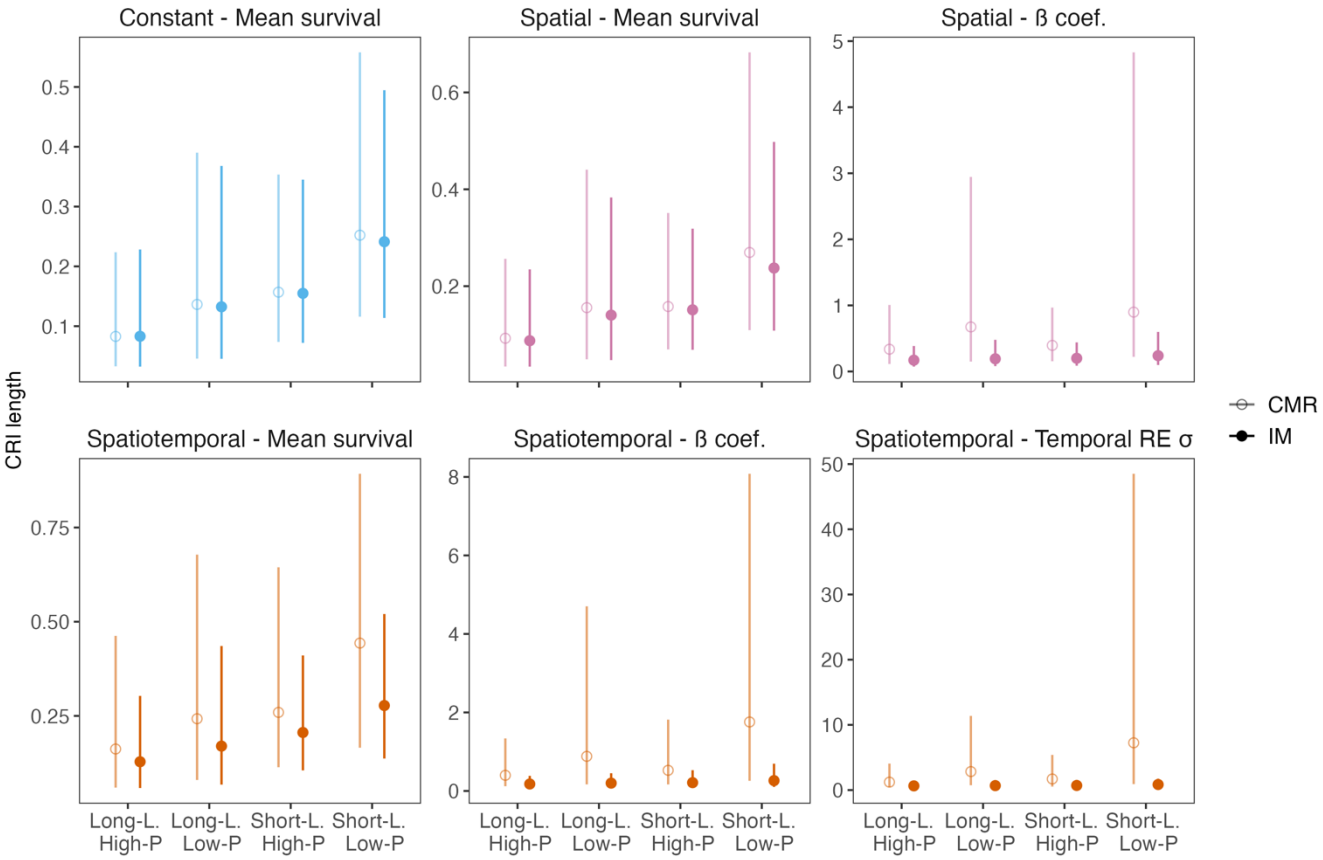
Constant - Mean survival
Spatial - Mean survival
Spatial - ß coef.
Spatiotemporal - Mean survival
Spatiotemporal - ß coef.
Spatiotemporal - Temporal RE σ
CRI length
CMR
IM
Long-L. High-P
Long-L. Low-P
Short-L. High-P
Short-L. Low-P

**Figure 4**

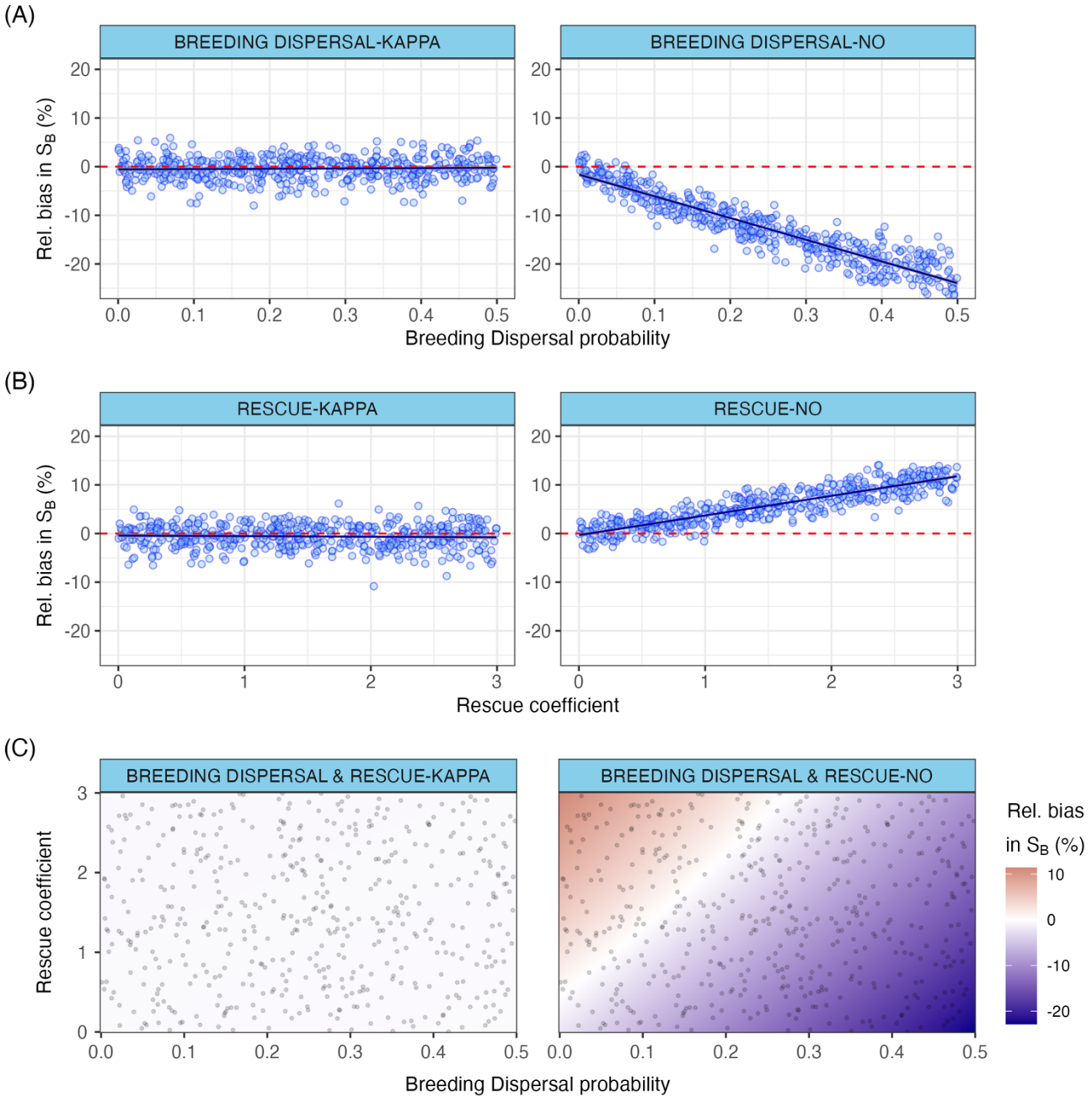
(A)
BREEDING DISPERSAL-KAPPA
BREEDING DISPERSAL-NO
Rel. bias in $S_B$ (%)
Breeding Dispersal probability
(B)
RESCUE-KAPPA
RESCUE-NO
Rel. bias in $S_B$ (%)
Rescue coefficient
(C)
BREEDING DISPERSAL & RESCUE-KAPPA
BREEDING DISPERSAL & RESCUE-NO
Rescue coefficient
Breeding Dispersal probability
Rel. bias in $S_B$ (%)
10
0
-10
-20

**Figure 5**

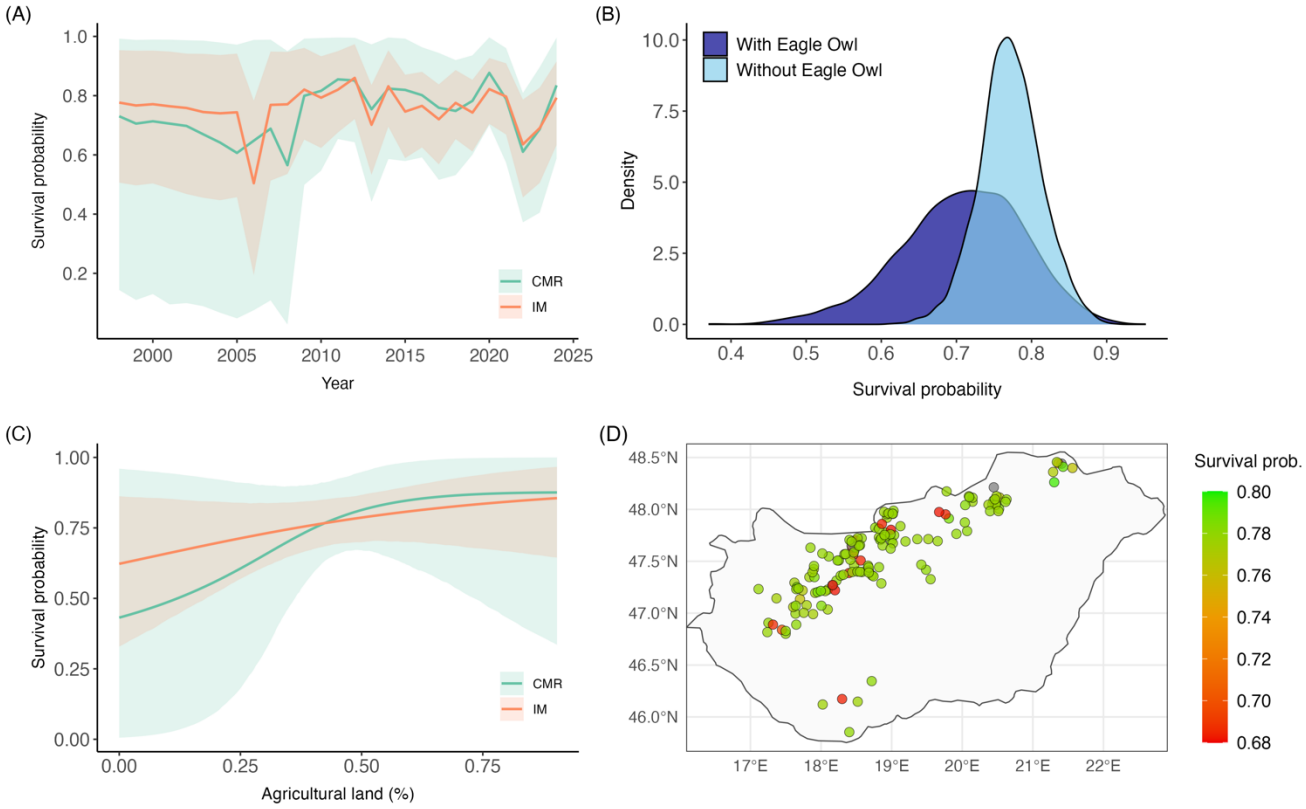
(A)
Survival probability
1.0
0.8
0.6
0.4
0.2
2000
2005
2010
2015
2020
2025
Year
CMR
IM
(B)
With Eagle Owl
Without Eagle Owl
Density
10.0
7.5
5.0
2.5
0.0
0.4
0.5
0.6
0.7
0.8
0.9
Survival probability
(C)
Survival probability
1.00
0.75
0.50
0.25
0.00
0.00
0.25
0.50
0.75
Agricultural land (%)
CMR
IM
(D)
48.5°N
48.0°N
47.5°N
47.0°N
46.5°N
46.0°N
17°E
18°E
19°E
20°E
21°E
22°E
Survival prob.
0.80
0.78
0.76
0.74
0.72
0.70
0.68

**Appendix S1**

**Methods**

Relaxing the persistence-survival relationship by introducing a scaling parameter, "$\kappa$"

In the main manuscript, for clarity of presentation, link functions are omitted from the equations illustrating the state process of the joint likelihood. In the models as actually implemented, though, time-varying persistence $\phi_t$ is expressed on the logit and $\kappa$ on the log scale, so that $\kappa$ acts multiplicatively on the odds of persistence – ensuring that persistence remains within the (0,1) range (Equation S1).

$$z_{s,t} \sim Bernoulli\left(z_{s,t-1} \cdot logit^{-1}\left(\log\left(\frac{\phi_t}{1-\phi_t} \cdot \kappa\right)\right) + \left(1 - z_{s,t-1}\right) \cdot \gamma_{s,t}\right)$$

*Equation S11*

Simulation study 1: bias, coverage, and precision gains of the integrated model under different survival structures

Description of the simulations

We initialized the population in year 1 by setting an initial number of breeders equal to half of the total number of available breeding sites. Each breeder was randomly assigned to one site. We additionally set the initial number of newborn individuals, which we obtained using random Poisson draws from the product of the initial number of breeders and the productivity rate set for that simulation, which we divided by two to obtain the number of

females, assuming an even sex ratio (Schaub & Kéry, 2022). Furthermore, in scenarios that involved the simulation of a long-lived species (See "Simulation scenario 2: Life history), we set an initial number of one-year-old individuals, all still nonbreeders, calculated as half of the number of initial breeders, and rounded to the next integer.

In subsequent years, demographic processes were simulated sequentially. First, we modelled survival for each individual using Bernoulli trials. If a breeder died, we set its site as empty and thus available to receive a new recruit in the following year. Individuals then aged by one year, and those reaching the age of first breeding were each assigned at random to one of the available sites. Last in each yearly step, we modelled reproduction for each breeder, with the number of fledglings drawn from a Poisson distribution with a specified mean productivity. For simplicity, and to prevent having to model density dependent processes in case of population saturation or quasi-extinction, we discarded simulations where sites became either all occupied or all empty.

For every simulation, we extracted three datasets: a) CMR encounter histories, b) a $\delta$ vector indicating the known breeding site of all individuals that were breeders, and c) a site-occupancy data matrix. We implemented imperfect detection in the CMR data via detection probabilities specified in the simulation. Likewise, the $\delta$ vector was subject to imperfect detection: breeding sites were recorded only for individuals ever observed breeding, while site identity was set as a missing value for individuals never detected as breeders. Occupancy data were assumed to be perfectly detected if a site was indeed visited; however, we included a visitation probability < 1: sites not visited in a given year were recorded as missing values in the occupancy matrix. We randomly selected a visitation probability

between 0.6 and 1 in 0.1 steps (0.6, 0.7, 0.8, 0.9, 0.1) at each simulation for realism purposes.

Scenario 1: Survival structure

For (i) the constant survival scenario, we simulated breeder survival as constant across sites and years. For (ii) the spatial survival scenario, we modelled breeder survival as depending on a site-level covariate. To add some realistic variability to the simulations, we let the regression coefficients of this covariate vary randomly between the values of -0.7 and 0.7 on the logit scale. We selected these values after initial tests to make sure they provided realistic levels of variation of survival across sites (max. of ca. $\mp 0.2$ around the mean). For (iii) the spatiotemporal scenario, we added annual Gaussian random effects with a temporal variance of 0.4 on the logit scale, which was again selected as it provided realistically looking interannual variation in survival.

Scenario 2: Life history

To assess model performance across different life histories, we conducted simulations for a hypothetical long-lived and a short-lived species. For the long-lived species, we set the age of first breeding at two years, and structured survival into three age classes: juveniles (from birth to their first year of age), subadults (from their first to their second year) and adults or breeders (two years and older). We set juvenile survival at 0.3, and subadult and adult survival at 0.8. We structured detection probability into two age classes: juveniles vs. older individuals. Productivity was set at 1.65 fledglings per breeding female and year assuming an equal sex ratio, hence resulting in 0.825 female fledglings per breeding female and year.

For the short-lived species, we set the age of first breeding at one year, with two survival classes: juveniles (0.2) and adults or breeders (0.5). We set detection probability as constant across ages, and we fixed productivity at 4.8 fledglings per breeding female and year, resulting in 2.4 female fledglings per breeding female and year. We selected the parameter values for both life histories so that they resulted in about the same number of increasing and decreasing population trajectories, again to make our simulation more general and realistic.

Scenario 3: Detection probability

To evaluate the effect of detection probability of marked breeders on model performance, we simulated all scenarios under two detection scenarios: high detection (0.7) and low detection (0.2). For the long-lived species, we fixed detection probabilities of nonbreeders at 0.1 in all scenarios to realistically represent the likely lower detection probabilities of nonbreeders (Badia-Boher et al., 2023).

Description of CMR models

We fitted Cormack-Jolly-Seber (CJS) models to the CMR subset of each simulated data scenario to compare the accuracy and precision of their estimates to those of the integrated models. The CJS models matched the survival structure used in the CJS submodel of the corresponding integrated models. All models were implemented using a marginalized CJS likelihood identical to that described in the main text (Schaub & Badia-Boher, 2025).

In all scenarios, survival and detection were structured by age class, with the total number of age classes depending on the life cycle of the modelled species (See “Simulation scenario

2: Life history"). Juvenile and subadult survival were modelled as spatially homogeneous in all scenarios, so differences in survival structures again referred to the structure imposed on breeder survival.

In (i) the constant survival model, breeder survival was assumed constant across space and time.

In (ii) the spatial survival model, we assigned every breeding individual to a specific site in the same way as we did in the integrated model, using the vector $\delta$. We allowed survival to vary by territory as a function of a continuous covariate $x$ and linked it to individual survival $S'$ via vector $\delta$.

$$logit(S_{B_s}) = \alpha + \beta \cdot x_s$$

*Equation S12*

$$S'_{B_i} = S_{B_{\delta_i}}$$

*Equation S13*

In (iii) the spatiotemporal survival model, breeder survival additionally varied over time. As in the integrated formulation, the model extended the spatial formulation by adding annual random effects.

$$logit\left(S_{B_{s,t}}\right) = \alpha + \beta \cdot x_s + \epsilon_t;\ \epsilon_t \sim Normal(0, \sigma)$$

*Equation S14*

$$S'_{B_{i,t}} = S_{B_{\delta_i,t}}$$

*Equation S15*

We specified the same priors as for the equivalent parameters in the integrated model (see Main Manuscript, "Statistical inference and model fitting").

Simulation study 2: The role of the scaling parameter $\kappa$ in ensuring unbiased survival estimates

This simulation study evaluated whether the scaling parameter $\kappa$ helps to produce unbiased estimates of survival when the assumption of a deterministic demographic link between breeder survival and site persistence was violated. All simulations were based on the same individual-based population model as in Simulation study 1. We simulated a long-lived species with constant survival and high mark-recapture detection probability.

To induce a controlled discrepancy between persistence and its demographic decomposition (Equation 3), we performed simulations under three scenarios.

In (i) the breeding dispersal scenario, we introduced breeding dispersal by allowing established breeders to relocate annually to a different empty territory with a given probability. This probability varied randomly across simulated datasets according to a Uniform(0, 0.5) distribution . Breeding dispersal was simulated after simulating survival and the acquisition of a territory by new breeders, but before productivity. Because breeding dispersal generates site turnover that is not related to mortality of a site owner, this mechanism reduces site persistence relative to what is expected from survival alone, and therefore induces values of $\kappa < 1$.

In (ii) the modified rescue dynamics scenario, we altered rescue dynamics such that recently vacated sites were more likely to be re-colonized by individuals reaching the age of first breeding than were sites that had been empty for $\geq 1$ time step. Under standard assumptions in our simulations, all unoccupied sites have equal probability of being acquired by first-time breeders. Here, instead, the selection probability of sites vacated at occasion *t* due to mortality of the previous territory holder received an additive term on the logit scale, that was drawn randomly from a Uniform(0, 3) distribution in each simulated dataset. Site selection probabilities were then normalized to sum to one across all sites. This preferential replacement inflates site persistence probability relative to the expectation based on survival alone and therefore induces a value of $\kappa > 1$.

In (iii) the model that combined breeding dispersal and altered rescue dynamics, we modelled both processes simultaneously to evaluate whether unbiased survival estimates were ensured by the introduction of $\kappa$ even when both processes were present. For each simulated dataset, we drew a breeding dispersal probability as described in scenario (i), and

a logit-scale additive term for a rescue effect as described in scenario (ii). We expected the value of $\kappa$ to vary depending on the relative strengths of the two processes in each dataset.

For each scenario, we fitted two versions of the integrated model: first, the integrated model we described above, and second, another model where $\kappa$ was removed from the formulation (Equation S6). Comparing survival estimates between both model formulations allowed us to test whether the inclusion of $\kappa$ resulted in unbiased survival estimates, and to illustrate potential biases in breeder survival if the scaling factor $\kappa$ is not introduced in the model.

$$z_{s,t} \sim Bernoulli\left(z_{s,t-1} \cdot (S_B + (1 - S_B) \cdot \gamma_t) + \left(1 - z_{s,t-1}\right) \cdot \gamma_t\right),$$

*Equation S16*

We simulated 500 datasets under the breeding dispersal scenario and 500 under the rescue effect scenario. Each dataset was analyzed with all three model formulations, resulting in 1500 simulated datasets and 3000 fitted models.

## Case study: Spatial patterns in the survival of Hungarian peregrine falcons

### i) Study area and population monitoring

The peregrine falcon became extinct in Hungary in the 1960s during the pesticide crash (Ratcliffe, 1993) and recolonized the country as late as 1997. Since then, the population increased steadily to 122 breeding pairs in 2023 and has been closely monitored by the *Peregrine Conservation Working Group Program*, managed by MME-BirdLife Hungary.

Monitoring efforts in the country included mark-resighting schemes and annual near-complete surveys of the occupancy of every breeding site. The mark-resighting program started when the first breeding pair established and has been running ever since, as have the occupancy surveys. Individuals were ringed with both metal and alphanumeric color rings. Resighting efforts were mostly devoted to breeding adults at nesting sites, but juveniles and immatures away from the breeding areas were also occasionally resighted. Live resighting efforts were restricted to Hungary, while dead recoveries of ringed birds were reported in Hungary and abroad, thus allowing us to estimate true survival (Burnham, 1993). A total of 893 individuals were ringed, of which 104 (11.6%) were resighted alive at least once, 61 (6.8%) were resighted as breeders, and 23 (2.6%) were recovered dead.

The occupancy status of breeding sites was monitored during every breeding season since 1997: sites occupied in previous years were visited one to three times in each breeding season to ascertain occupancy. In addition, previously unoccupied sites with suitable cliffs were prospected each year. Unfortunately, the resulting replicated detection/nondetection data were aggregated by year, preventing us from explicitly modelling imperfect detection in the observation process. However, given the relatively high detection probability of this species (Kéry & Royle, 2016) and the small dimensions of most breeding cliffs in Hungary we consider the assumption of near-perfect detection reasonable and therefore that its ignorance in our model would not materially affect our inferences.

ii) Model definition

We formulated the integrated model as the spatiotemporal case described in the Methods. The only difference concerns the CMR component, which was specified as a multistate model, rather than a Cormack-Jolly-Seber (CJS) model (Schaub & Kéry, 2022), to simultaneously analyse both dead recovery and life resighting data. This modification did not alter the joint likelihood or the persistence process.

$$z_{s,t} \sim Bernoulli\left(z_{s,t-1} \cdot \left(S_{B_{s,t}} + \left(1 - S_{B_{s,t}}\right) \cdot \gamma_t\right) \cdot \kappa + \left(1 - z_{s,t-1}\right) \cdot \gamma_t\right)$$

*Equation S17*

We modelled breeder survival $S_{B_{s,t}}$ as a function of two site-level covariates and a random effect of the year:

$$logit\left(S_{B_{s,t}}\right) = \alpha + \beta_1 \cdot x_{EO_s} + \beta_2 \cdot x_{A_{s,t}} + \epsilon_t,$$

*Equation S18*

where $\alpha$ is the intercept, $\beta_1$ and $\beta_2$ are regression coefficients. Covariate $x_{EO}$ is binary and indicates the presence of a historic eagle-owl territory (i.e., known and occupied at any time between 2014 and 2024, the period for which eagle owl data are available) within a 2 km radius of a peregrine falcon territory. Even if there is no eagle owl data available before 2014, we assumed that eagle owl territories were present at the same locations since the beginning of the study in 1997, a reasonable assumption considering the strong territory fidelity of the species over the years (Penteriani & Delgado, 2019). Covariate $x_A$ is continuous and indicates the proportion of the peregrine territory occupied by agricultural land. This

proportion was calculated using arable surface information from CORINE land cover data and a buffer with a radius of 4 km around each nest location as the approximate territory size, following the same procedure as described in Prommer et al. (2026).

Finally, $\epsilon_t$ is the yearly random effect governed by:

$$\epsilon_t \sim Normal(0, \sigma)$$

*Equation S19*

Site-level survival $S_{B_{s,t}}$ was linked to individual-level survival $S'_{B_{i,t}}$ through vector $\delta$, which stores the breeding site of every individual as described in the *Methods* section of the main manuscript (Figure 1, Equations 6-7). Likewise, as shown earlier, the identity of the breeding site (i.e., the value of $\delta$) is known only for individuals that are observed breeding at least once. For individuals never observed breeding, $\delta_i$ was treated as a discrete latent variable drawn from the set of all sites in the occupancy dataset.

We developed a multistate model that combined live resightings and dead recoveries (Burnham, 1993) implemented via a marginalized state-space likelihood (Schaub & Badia-Boher 2025). We assumed that individuals start breeding at the age of two years. The states represented age classes and the live/dead status. Namely, $A_J$ stood for "Alive as a juvenile", $A_{B1}$ for "Alive as a first-year breeder", $A_B$ for "Alive as a breeder", $D$ for "Dead", and $LD$ for "Long Dead". We defined the observed states as: "Seen alive as a juvenile" (1), "Seen alive as a first-year breeder" (2), "Seen alive as a breeder" (3), "Recovered dead" (4), and "Not Seen or not recovered" (5). We assume that dead individuals can only be recovered during

the occasion of death according to a recovery probability *r*, as is typically done in models that include dead recoveries (Burnham, 1993).

We defined detection probability $p$ to be constant in space and time, but varying by age class, with $p_J$ as the first year and $p_B$ as the breeder detection probability, respectively. We modelled the recovery probability $r$ as a constant. Individual survival probabilities were also structured by age class. For simplicity, we defined individual juvenile survival probability $S_J$ as constant over space and time. $S'_{B_{i,t}}$ was the survival probability of two-year-old and older individuals (i.e., breeders).

We formulated a state transition matrix $\zeta$ that defined transitions between states across consecutive occasions governed by survival parameters, and an observation matrix $\Omega$ that defined the mapping of the true latent states onto the observed states within each occasion, and which was governed by detection and recovery parameters (Schaub & Kéry, 2022).

| | $\boldsymbol{A_J}$ | $\boldsymbol{A_{B1}}$ | $\boldsymbol{A_B}$ | $\boldsymbol{D}$ | $\boldsymbol{LD}$ |
|---|---|---|---|---|---|
| $\boldsymbol{A_J}$ | $0$ | $S_J$ | $0$ | $1 - S_J$ | $0$ |
| $\boldsymbol{A_{B1}}$ | $0$ | $0$ | $S'_{B_{i,t}}$ | $1 - S'_{B_{i,t}}$ | $0$ |
| $\boldsymbol{A_B}$ | $0$ | $0$ | $S'_{B_{i,t}}$ | $1 - S'_{B_{i,t}}$ | $0$ |
| $\boldsymbol{D}$ | $0$ | $0$ | $0$ | $0$ | $1$ |
| $\boldsymbol{LD}$ | $0$ | $0$ | $0$ | $0$ | $1$ |

*Equation S10. Transition matrix $\zeta$. Rows denote the state at occasion t, and columns denote the state at occasion t+1.*

| | **1** | **2** | **3** | **4** | **5** |
|---|---|---|---|---|---|
| $\boldsymbol{A_J}$ | 0 | 0 | 0 | 0 | 1 |
| $\boldsymbol{A_{B1}}$ | 0 | $p_J$ | 0 | 0 | $1-p_J$ |
| $\boldsymbol{A_B}$ | 0 | 0 | $p_B$ | 0 | $1-p_B$ |
| $\boldsymbol{D}$ | 0 | 0 | 0 | $r$ | $1-r$ |
| $\boldsymbol{LD}$ | 0 | 0 | 0 | 0 | 1 |

*Equation S11. Observation matrix $\Omega$. Rows denote the state at occasion t, and columns denote observation at occasion t.*

For comparison, we fitted a multistate CMR-only model with the same structure as that in the integrated model, but excluding the occupancy component.

We assigned the same priors as the ones used in the simulations for each parameter (see main manuscript: *Statistical inference and model fitting*). The only modification concerned the latent scaling parameter $\kappa$, for which we increased the upper limit of the uniform prior distribution to 10 to accommodate potentially larger values in the real-case application.

**References**

Badia-Boher, J.A., Real, J., Riera, J.L., Bartumeus, F., Parés, F., Bas, J.M., & Hernández-Matías, A. (2023). Joint estimation of survival and dispersal effectively corrects the permanent emigration bias in mark-recapture analyses. *Scientific Reports*, 13, 6970.

Burnham, K.P. (1993). A theory for combined analysis of ring recovery and recapture data. In J.D. Lebreton & P.M. North (Eds.), *Marked individuals in the study of bird populations* (pp. 199-213). Birkhäuser Verlag.

Hernández-Matías, A., Real, J., & Pradel, R. (2011). Quick methods for evaluating survival of age-characterizable long-lived territorial birds. *The Journal of Wildlife Management*, *75*(4), 856–866.

Kéry, M., & Royle, J.A. (2016). *AHM1 – Modeling distribution, abundance and species richness using R and BUGS. Volume 1: Prelude and Static Models*. Academic Press.

Kéry, M., Monneret, R.-J., Badia-Boher, J.-A., & Schaub, M. (2025). Demographic causes of the pesticide crash in the peregrine falcon. *Ecoevorxiv*, *https://doi.org/10.32942/X2R05B*

Penteriani, V., & Delgado, M.M. (2019). *The Eagle Owl*. T & AD Poyser.

Prommer, M., Bagyura, J., Kéry, M., & Oli, M.K. (2026). Repopulation of the former breeding range: spatio-temporal patterns and drivers of reproduction in the Peregrine Falcon (Falco peregrinus) population in Hungary. *Ibis*, 168, 63-78.

Ratcliffe, D. A. (1993). *The peregrine falcon*. T & AD Poyser.

Roth, T., & Amrhein, V. (2010). Estimating individual survival using territory occupancy data on unmarked animals. *Journal of Applied Ecology*, *47*(2), 386–392.

Schaub, M., & Kéry, M. (2022). *Integrated population models: Theory and ecological applications with R and JAGS*. Academic Press.

Schaub, M., & Badia-Boher, J.A. (2025). Comparison of Bayesian Models to Estimate Survival From Dead-Recovery Alone and Together With Live-Encounter Data: Challenges and Opportunities. *Ecology and Evolution*, *15*(6), e71517.

**Figures**

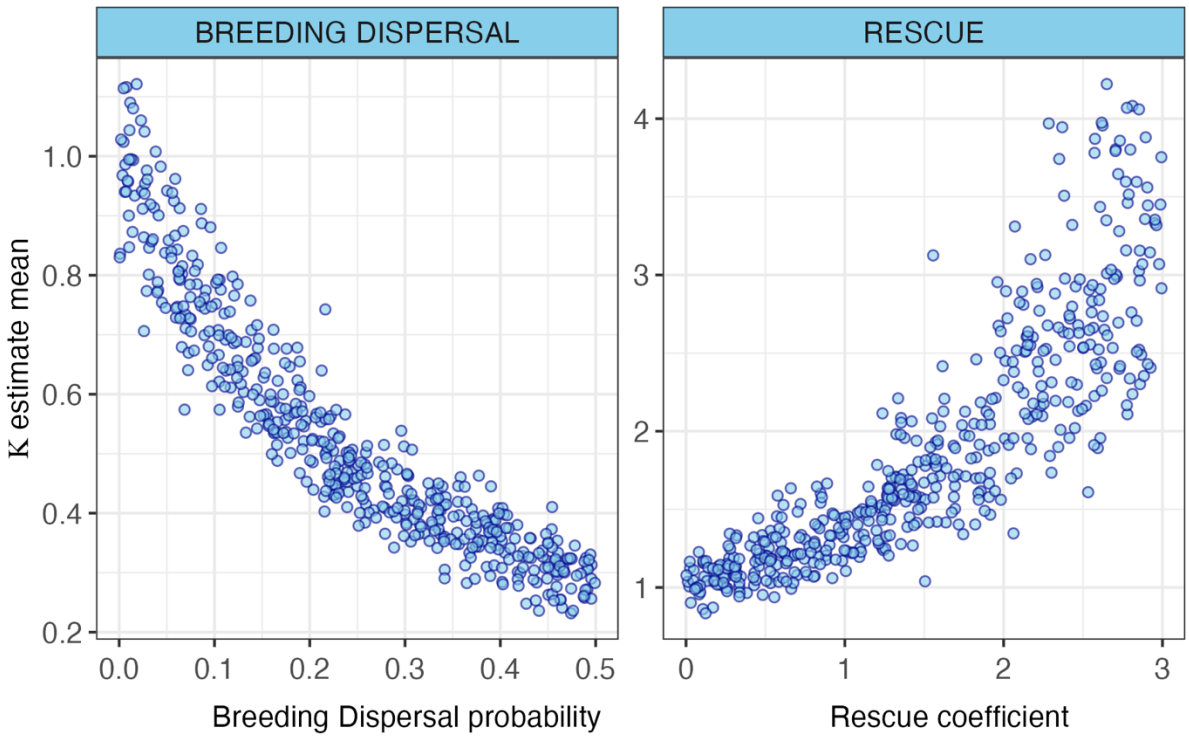


Figure S1. Posterior means of $\kappa$ estimates under increasing breeding dispersal probabilities (left) or strength of the rescue effect (right).

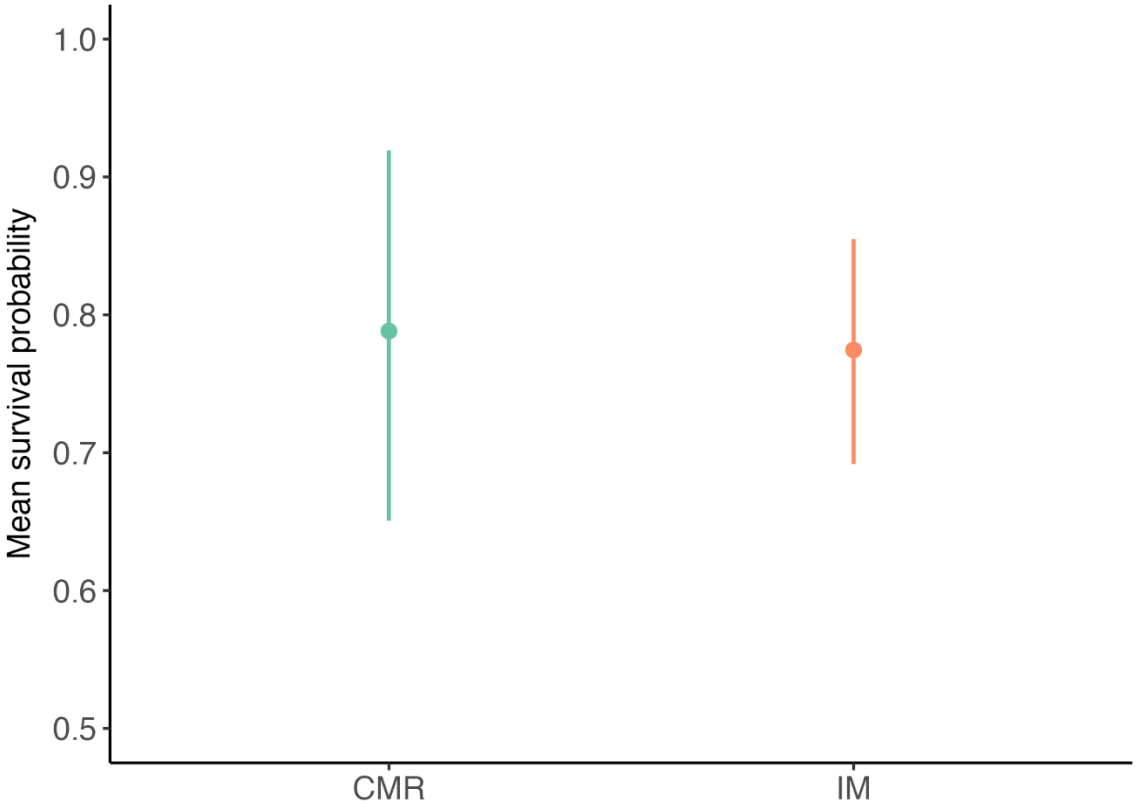


Figure S2. Posterior means and 95% credible intervals of the hypermean of survival probability of breeders in capture-mark-recapture-only (CMR) and integrated models (IM) for the case study of Hungarian peregrine falcons.

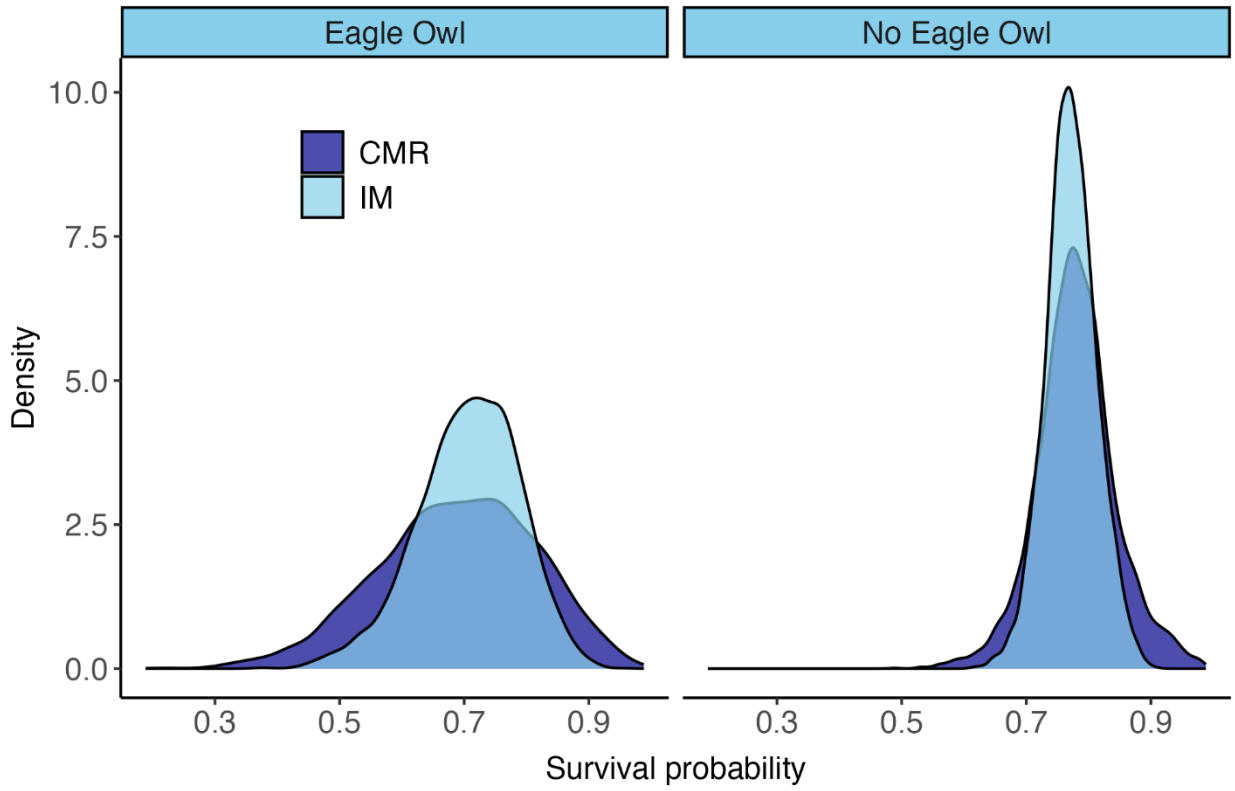


Figure S3. Posterior distributions of mean breeder survival probability under presence vs absence of eagle owl territories for capture-mark-recapture-only (CMR) and integrated models (IM).

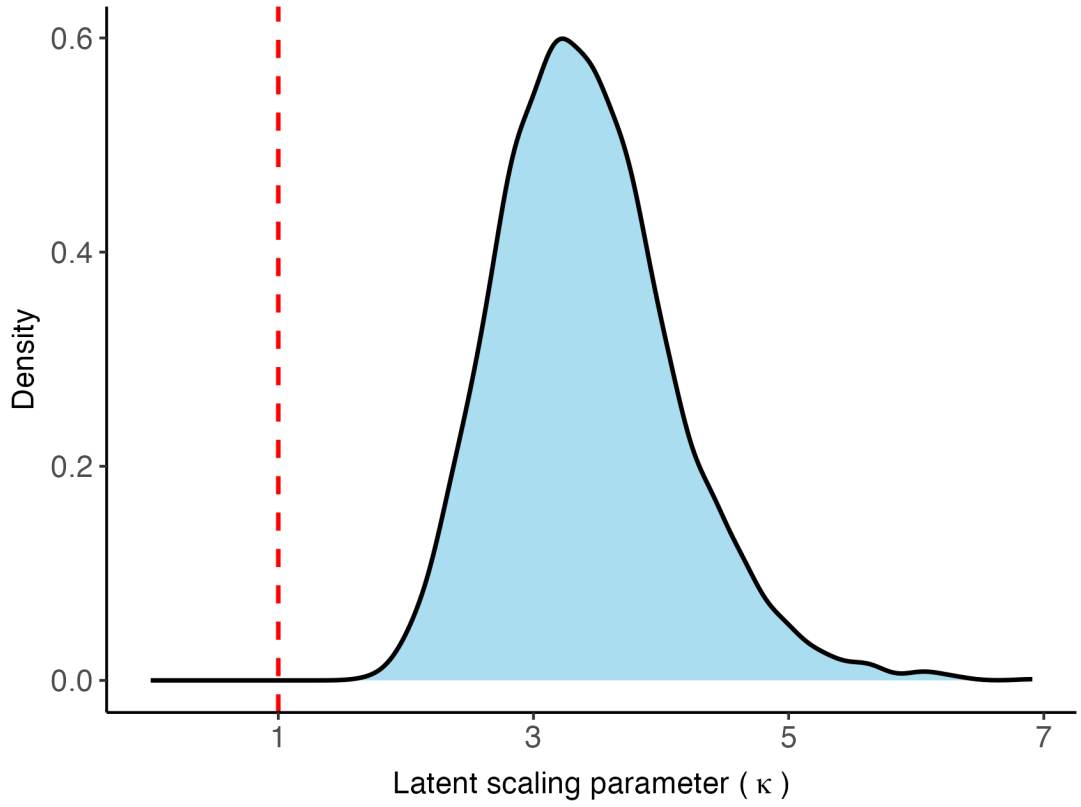


Figure S4. Posterior distribution of $\kappa$ in the peregrine falcon case study, based on the integrated model. The dashed line indicates $\kappa = 1$, the value that would indicate no mismatch between site-level persistence and its deterministic demographic decomposition.

## Tables

| Constant Survival Models | | | |
|---|---|---|---|
| **Parameter** | **Rel. Bias (%, Median $\pm$ 95%)** | **CRI length (Mean $\pm$ 95%)** | **Coverage** |
| **Long-Lived – High detection** | | | |
| $\kappa$ | 1.6 (-18.5, 45.4) | 0.645 (0.265, 1.892) | 0.988 |
| $\gamma$ | 4.6 (-28.6, 58.2) | 0.181 (0.094, 0.369) | 0.996 |
| $S_B$ Mean | -0.4 (-8.9, 4.2) | 0.083 (-6.227, 5.732) | 0.938 |
| **Long-Lived – Low detection** | | | |
| $\kappa$ | 3.8 (-30.5, 86.5) | 0.952 (0.327, 3.159) | 0.970 |
| $\gamma$ | 4.6 (-28.1, 58.3) | 0.181 (0.095, 0.366) | 0.996 |
| $S_B$ Mean | -0.8 (-15.1, 6.7) | 0.132 (-6.674, 11.471) | 0.938 |
| **Short-Lived – High detection** | | | |
| $\kappa$ | 1.4 (-22.2, 45.3) | 0.646 (0.295, 1.469) | 0.962 |
| $\gamma$ | 2.1 (-22.8, 42.0) | 0.177 (0.086, 0.341) | 0.994 |
| $S_B$ Mean | -1.0 (-20.8, 13.9) | 0.155 (-4.933, 6.249) | 0.944 |
| **Short-Lived – Low detection** | | | |
| $\kappa$ | -2.6 (-27.2, 104.2) | 0.975 (0.404, 2.842) | 0.950 |
| $\gamma$ | 2.2 (-23.0, 42.4) | 0.177 (0.086, 0.340) | 0.993 |
| $S_B$ Mean | -1.6 (-37.7, 21.0) | 0.241 (-4.409, 12.030) | 0.940 |

Table S1. Relative Bias (%), credible interval ("CRI") length, and coverage of different parameters, life histories, and capture-mark-recapture detection scenarios for constant survival models.

| | Spatial Survival Models | | |
|---|---|---|---|
| **Parameter** | **Rel. Bias (%, Median $\pm$ 95%)** | **CRI length (Mean $\pm$ 95%)** | **Coverage** |
| **Long-Lived – High detection** | | | |
| $\boldsymbol{\beta}$ | -1.1 (-67.6, 124.5) | 0.171 (0.073, 0.385) | 0.910 |
| $\boldsymbol{\kappa}$ | 1.2 (-21.4, 43.8) | 0.655 (0.272, 1.939) | 0.988 |
| $\boldsymbol{\gamma}$ | 4.7 (-26.8, 58.7) | 0.180 (0.099, 0.360) | 0.997 |
| $\boldsymbol{S_B}$ **Mean** | -0.4 (-8.8, 4.8) | 0.087 (-4.243, 17.064) | 0.948 |
| **Long-Lived – Low detection** | | | |
| $\boldsymbol{\beta}$ | -3.5 (-99.5, 122.2) | 0.192 (0.081, 0.479) | 0.922 |
| $\boldsymbol{\kappa}$ | 1.8 (-32.1, 113.0) | 0.992 (0.331, 3.274) | 0.964 |
| $\boldsymbol{\gamma}$ | 4.7 (-26.9, 58.9) | 0.180 (0.099, 0.359) | 0.996 |
| $\boldsymbol{S_B}$ **Mean** | -0.5 (-20.7, 7.3) | 0.140 (-4.806, 26.680) | 0.936 |
| **Short-Lived – High detection** | | | |
| $\boldsymbol{\beta}$ | 0.1 (-67.3, 117.7) | 0.200 (0.087, 0.440) | 0.926 |
| $\boldsymbol{\kappa}$ | 1.9 (-22.7, 37.1) | 0.606 (0.270, 1.510) | 0.960 |
| $\boldsymbol{\gamma}$ | 1.0 (-21.5, 34.7) | 0.196 (0.106, 0.358) | 0.976 |
| $\boldsymbol{S_B}$ **Mean** | -0.9 (-21.3, 12.9) | 0.151 (-3.947, 13.065) | 0.948 |
| **Short-Lived – Low detection** | | | |
| $\boldsymbol{\beta}$ | 0.1 (-112.4, 130.7) | 0.239 (0.098, 0.599) | 0.952 |
| $\boldsymbol{\kappa}$ | 3.9 (-31.9, 69.1) | 0.872 (0.358, 2.417) | 0.958 |
| $\boldsymbol{\gamma}$ | 1.0 (-21.7, 35.1) | 0.196 (0.107, 0.355) | 0.977 |
| $\boldsymbol{S_B}$ **Mean** | -1.7 (-36.3, 23.0) | 0.237 (-2.707, 34.496) | 0.954 |

Table S2. Relative Bias (%), credible interval ("CRI") length, and coverage of different parameters, life histories, and capture-mark-recapture detection scenarios for spatial survival models.

| | Spatiotemporal Survival Models | | |
|---|---|---|---|
| **Parameter** | **Rel. Bias (%, Median $\pm$ 95%)** | **CRI length (Mean $\pm$ 95%)** | **Coverage** |
| **Long-Lived – High detection** | | | |
| $\boldsymbol{\beta}$ | -0.1 (-117.3, 134.2) | 0.178 (0.075, 0.385) | 0.892 |
| $\boldsymbol{\kappa}$ | 1.8 (-19.8, 64.7) | 0.714 (0.276, 2.194) | 0.986 |
| $\boldsymbol{\gamma}$ | 5.0 (-27.4, 58.5) | 0.175 (0.084, 0.352) | 0.998 |
| $\boldsymbol{S_B}$ **Mean** | -0.8 (-14.0, 5.5) | 0.128 (-35.789, 50.733) | 0.964 |
| $\boldsymbol{S_{B_t}}$ | -0.6 (-14.0, 13.0) | 0.181 (-22.494, 63.480) | 0.929 |
| $\boldsymbol{\sigma}$ | 13.4 (-50.3, 99.8) | 0.645 (-6.782, 72.545) | 0.936 |
| **Long-Lived – Low detection** | | | |
| $\boldsymbol{\beta}$ | -1.1 (-123.5, 113.8) | 0.199 (0.084, 0.451) | 0.896 |
| $\boldsymbol{\kappa}$ | 2.4 (-30.1, 120.6) | 1.034 (0.334, 3.415) | 0.954 |
| $\boldsymbol{\gamma}$ | 5.0(-27.8, 58.6) | 0.175 (0.084, 0.354) | 0.998 |
| $\boldsymbol{S_B}$ **Mean** | -0.8 (-19.6, 6.3) | 0.170 (-14.036, 56.893) | 0.940 |
| $\boldsymbol{S_{B_t}}$ | -0.8 (-17.5, 15.2) | 0.214 (-6.395, 71.811) | 0.932 |
| $\boldsymbol{\sigma}$ | 3.4 (-54.7, 96.8) | 0.683 (38.130, 92.287) | 0.970 |
| **Short-Lived – Large detection** | | | |
| $\boldsymbol{\beta}$ | 1.1 (-145.3, 117.1) | 0.212 (0.093, 0.529) | 0.908 |
| $\boldsymbol{\kappa}$ | -0.4 (-24.3, 48.7) | 0.650 (0.280, 1.640) | 0.970 |
| $\boldsymbol{\gamma}$ | 1.9 (-22.7, 39.0) | 0.196 (0.086, 0.376) | 0.987 |
| $\boldsymbol{S_B}$ **Mean** | -1.5 (-27.1, 17.0) | 0.206 (-31.561, 51.056) | 0.944 |
| $\boldsymbol{S_{B_t}}$ | 1.1 (-32.8, 38.4) | 0.298 (-13.351, 56.345) | 0.936 |
| $\boldsymbol{\sigma}$ | 9.7 (-57.7, 102.6) | 0.705 (-4.175, 80.970) | 0.956 |
| **Short-Lived – Low detection** | | | |
| $\boldsymbol{\beta}$ | 1.2 (-120.5, 160.4) | 0.264 (0.103, 0.694) | 0.898 |
| $\boldsymbol{\kappa}$ | 6.8 (-28.4, 74.7) | 0.940 (0.356, 2.400) | 0.952 |
| $\boldsymbol{\gamma}$ | -1.9 (-23.3, 40.2) | 0.197 (0.085, 0.377) | 0.987 |
| $\boldsymbol{S_B}$ **Mean** | -5.0 (-38.7, 20.8) | 0.278 (-10.760, 65.070) | 0.946 |
| $\boldsymbol{S_{B_t}}$ | -3.8 (-42.0, 40.7) | 0.354 (12.613, 67.265) | 0.935 |
| $\boldsymbol{\sigma}$ | -7.9 (-55.0, 132.8) | 0.850 (34.018, 98.107) | 0.964 |

Table S3. Relative Bias (%), credible interval ("CRI") length, and coverage of different parameters, life histories, and capture-mark-recapture detection scenarios for spatiotemporal survival models.

| | CRI length | | |
|---|---|---|---|
| | **IM (Mean ± 95%)** | **CMR (Mean ± 95%)** | **Gain in IM (%)** |
| **Constant – Survival Mean** | | | |
| Long-Lived - High detection | 0.083 (0.032, 0.228) | 0.083 (0.033, 0.224) | -0.2 |
| Long-Lived - Low detection | 0.132 (0.045, 0.368) | 0.136 (0.046, 0.390) | 2.9 |
| Short-Lived - High detection | 0.155 (0.072, 0.345) | 0.157 (0.074, 0.353) | 1.3 |
| Short-Lived - Low detection | 0.241 (0.114, 0.495) | 0.252 (0.116, 0.558) | 4.3 |
| **Spatial - Survival Mean** | | | |
| Long-Lived - High detection | 0.087 (0.034, 0.235) | 0.092 (0.034, 0.256) | 5.4 |
| Long-Lived - Low detection | 0.140 (0.047, 0.383) | 0.156 (0.049, 0.441) | 9.9 |
| Short-Lived - High detection | 0.151 (0.069, 0.319) | 0.158 (0.069, 0.351) | 4.3 |
| Short-Lived - Low detection | 0.237 (0.108, 0.498) | 0.270 (0.109, 0.683) | 11.9 |
| **Spatial - Survival Beta** | | | |
| Long-Lived - High detection | 0.171 (0.073, 0.385) | 0.337 (0.113, 1.006) | 49.3 |
| Long-Lived - Low detection | 0.192 (0.081, 0.479) | 0.674 (0.150, 2.945) | 71.6 |
| Short-Lived - High detection | 0.200 (0.087, 0.440) | 0.395 (0.155, 0.967) | 49.4 |
| Short-Lived - Low detection | 0.239 (0.098, 0.599) | 0.898 (0.222, 4.829) | 73.4 |
| **Spatiotemporal - Survival Mean** | | | |
| Long-Lived - High detection | 0.128 (0.059, 0.303) | 0.162 (0.060, 0.462) | 20.9 |
| Long-Lived - Low detection | 0.170 (0.068, 0.435) | 0.242 (0.080, 0.678) | 29.9 |
| Short-Lived - High detection | 0.206 (0.105, 0.410) | 0.259 (0.114, 0.644) | 20.6 |
| Short-Lived - Low detection | 0.278 (0.137, 0.520) | 0.443 (0.166, 0.893) | 37.4 |
| **Spatiotemporal - Survival Beta** | | | |
| Long-Lived - High detection | 0.178 (0.075, 0.385) | 0.399 (0.121, 1.339) | 55.5 |
| Long-Lived - Low detection | 0.199 (0.084, 0.451) | 0.882 (0.168, 4.703) | 77.4 |
| Short-Lived - High detection | 0.212 (0.093, 0.529) | 0.526 (0.167, 1.817) | 59.7 |
| Short-Lived - Low detection | 0.264 (0.103, 0.694) | 1.757 (0.259, 8.080) | 85.0 |
| **Spatiotemporal - Survival Sigma** | | | |
| Long-Lived - High detection | 0.645 (0.315, 1.382) | 1.218 (0.456, 4.062) | 47.0 |
| Long-Lived - Low detection | 0.683 (0.337, 1.537) | 2.838 (0.743, 11.370) | 75.9 |
| Short-Lived - High detection | 0.705 (0.355, 1.546) | 1.704 (0.539, 5.392) | 58.6 |
| Short-Lived - Low detection | 0.850 (0.379, 1.744) | 7.251 (0.921, 48.513) | 88.3 |
| **Spatiotemporal - Time-varying Survival** | | | |
| Long-lived - High detection | 0.181 (0.103, 0.344) | 0.266 (0.132, 0.591) | 31.9 |
| Long-lived - Low detection | 0.214 (0.115, 0.430) | 0.392 (0.192, 0.853) | 45.5 |
| Short-lived - High detection | 0.298 (0.198, 0.506) | 0.429 (0.237, 0.837) | 30.6 |
| Short-lived - Low detection | 0.354 (0.226, 0.592) | 0.657 (0.372, 1.000) | 46.1 |

Table S4. Credible interval ("CRI") lengths of main survival parameters under different survival structures, life histories, and capture-mark-recapture detection probabilities for integrated

models (IM) and capture-mark-recapture-only models (CMR). Column “Gain in IM” indicates the percentage of credible interval length reduction in integrated models compared to CMR models.